REPORT DOCUMENTATION PAGE

AFRL-SR-BL-TR-98-

0751

1. AGENCY USE ONLY (Leave Blank)	2. REPORT DATE	3. REPORT TYPE AND DATES COVERED
	August, 1994	Final

4. TITLE AND SUBTITLE
Isolation and Structure Elucidation of Bioactive Secondary Metabolites from Microbial Sources

5. FUNDING NUMBERS

6. AUTHORS
Kate J. Graham

7. PERFORMING ORGANIZATION NAME(S) AND ADDRESS(ES)
Cornell University

8. PERFORMING ORGANIZATION REPORT NUMBER

9. SPONSORING/MONITORING AGENCY NAME(S) AND ADDRESS(ES)
AFOSR/NI
4040 Fairfax Dr, Suite 500
Arlington, VA 22203-1613

10. SPONSORING/MONITORING AGENCY REPORT NUMBER

11. SUPPLEMENTARY NOTES

12a. DISTRIBUTION AVAILABILITY STATEMENT
Approved for Public Release

12b. DISTRIBUTION CODE

13. ABSTRACT *(Maximum 200 words)*
See attachment

14. SUBJECT TERMS

15. NUMBER OF PAGES

16. PRICE CODE

17. SECURITY CLASSIFICATION OF REPORT	18. SECURITY CLASSIFICATION OF THIS PAGE	19. SECURITY CLASSIFICATION OF ABSTRACT	20. LIMITATION OF ABSTRACT
Unclassified	Unclassified	Unclassified	UL

ISOLATION AND STRUCTURE ELUCIDATION OF BIOACTIVE SECONDARY METABOLITES FROM MICROBIAL SOURCES

A Dissertation

Presented to the Faculty of the Graduate School

of Cornell University

in Partial Fulfillment of the Requirements for the Degree of

Doctor of Philosophy

by

Kate J. Graham

August 1994

ISOLATION AND STRUCTURE ELUCIDATION OF BIOACTIVE SECONDARY METABOLITES FROM MICROBIAL SOURCES

Kate J. Graham, Ph.D.

Cornell University 1994

Microbial organisms often produce biologically active and chemically intriguing secondary metabolites. To isolate and characterize compounds of novel activity and structure, bioassay-guided fractionations were employed on a variety of natural products sources. Active compounds were characterized by spectroscopic analysis and X-ray diffraction methods.

As a result of these studies, six projects were completed, resulting in the purification of a diverse range of compounds containing activity in a variety of assays. A coumarin and para-hydroxyphenylethanol were determined to possess phytotoxic activity from fungal pathogens. Two novel C-glycosidic compounds from a bacterial plant pathogen were found to be the first low molecular weight elicitors of the hypersensitive response in plants. A verticillin of the epi-polythiodiketopiperazine class isolated from a soil fungus was discovered to be responsible for inhibition of *ras* farnesylation transferase. Leafcutter ants were found to be deterred by the presence of a novel sesquiterpenoid in epiphylls. Finally, inhibitors of the PDGF receptor were isolated and characterized from a lichen.

All of the compounds have potential uses as herbicides or pharmaceutical leads, but they also exemplify the information that can be gained through understanding the interactions of natural products with receptors in biological systems.

BIOGRAPHICAL SKETCH

The author was born January 3rd, 1967, in Long Beach, California, and was raised in southwestern Montana. She attended Montana State University, where she became involved in chemistry research in the laboratories of John H. Cardellina II and Larry Jackson. During the summers she twice participated in research projects at the National Institutes of Health, Bethesda, MD, working with Jim Omichinski and Peter Roller. She graduated with a B.S. degree in chemistry in 1989 and moved to Cornell University, where she joined the research group of Jon Clardy. She has accepted a faculty position at St. John's University / College of St. Benedict in Minnesota.

For My Father

ACKNOWLEDGEMENTS

I would like to acknowledge the Department of Defense, Air Force Office of Scientific Research and the Department of Education for fellowship support during this thesis work. In addition, I should thank Jon Clardy, my thesis advisor, for his leadership and guidance, and those faculty who served on my graduate committees: Barry Carpenter, Jerrold Meinwald, and Bruce Ganem. This work would not have been possible without the collaborative efforts of Ulrich Mueller, Steve Coval of Schering-Plough Corporation, Steve Krueger and Don Roberts of Boyce-Thompson Institute, Jim Sims of University of California, Riverside, and Gary Strobel of Montana State University. Invaluable experimental assistance was provided by Jorge L. Rios Steiner of the Cornell X-ray Diffraction Facility and by Dave Fuller and Aidan Harrison of the Cornell NMR Facility. The indispensible contribution of the Lynah Library to this work is greatly appreciated. Finally, I must thank the entire dark side of the Clardy group for many enjoyable conspiracies.

TABLE OF CONTENTS

LIST OF FIGURES

LIST OF TABLES

Chapter 1

Isolation and Structure of a Phytotoxin from *Phyllosticta sp.*

1.1 Introduction

All plants are hosts to many pathogens that induce disease symptoms by production of phytotoxins.[1] These pathogens are capable of destroying an entire crop when, as is common practice today, large areas of crop plants are in monoculture.[2] Such massive crop losses have become a serious economic problem, which has led plant pathologists to search for a method to develop resistant crops. Pathogens are often used to screen for these resistant cultivars. However, using pathogens themselves is often a problem due to culturing conditions and maintenance of the pathogen strains.[3] Thus, the isolation and structural characterization of phytotoxins is of considerable agricultural interest for their use as available screening agents.[1] These phytotoxins are useful tools not only for screening plants for toxin insensitivity (disease resistance) but also as probes to study normal plant molecular biochemistry.

For several plant pathogens, such as viruses and nematodes, there is no record of secondary metabolites being linked with the

diseases caused by these organisms. However, Fungi Imperfecti and bacteria are well known for the production of phytotoxic compounds. As fungal pathogens are diverse and are readily cultured, they are a good starting point for just such an application.[4]

Kenaf, or Thai green stem, is of importance as an agricultural fiber crop in Thailand as well as for its use in the reforestation of parts of Thailand. Unfortunately, this crop has been blighted by the attack of the fungal pathogen, *Phyllosticta sp.*, which is a host-specific pathogen to Kenaf, *Hibiscus sabdariffa var. altrissima.* The isolation and structural characterization of the phytotoxin from this fungal pathogen was undertaken.

1.2 Results and Discussion

Fermentation conditions were adjusted to maximize the production of the phytotoxin. *Phyllosticta sp.* was cultured on a dry sterile cornmeal/molasses medium for 30 days at room temperature. Stressing a microorganism with slow, nutrient-deficient growth conditions will often maximize toxin production.

The fungal culture was extracted with ethyl acetate and water several times. The biological activity, as determined by the leaf nick assay, was found to be contained in the organic fraction. Purification proceeded with column chromatography, first on a flash silica column with 1:1 hexane: ethyl acetate as the eluant. Upon bioassay-guided determination of the active fraction, further purification of this

fraction on a Sephadex LH-20 column with methanol as the eluent was carried out. Final fractionation was achieved on a reverse phase semipreparative HPLC column using a gradient from 50% acetonitrile in water to 100% acetonitrile over 25 minutes while monitoring at a wavelength at 214 nm.

The compound that was responsible for the phytotoxic activity on Kenaf caused large necrotic lesions when applied to the leaves of the plant. The spectroscopic data for this compound suggested a coumarin skeleton. The molecular formula was determined to be $C_{12}H_{12}O_5$ by high resolution mass spectrometry. The carbonyl band at 1710 cm^{-1} and the double bond absorptions at 1620 and 1590 cm^{-1} supports the proposed coumarin skeleton. The proton NMR spectrum showed *meta* related hydrogens at 6.5 ppm and 6.7 ppm, while the chemical shift of the singlet at 7.70 ppm was consistent with the shift of the proton present on the β-carbon of the double bond. Two singlets resonating at 3.90 ppm and 3.80 ppm indicated aromatic methoxy groups. A doublet at 4.6 ppm coupled to a broad triplet at 2.4 ppm seemed to support a hydroxymethyl substitution at the α-carbon. Two possible structures, **1** and **2**, were proposed for the phytotoxin (Figure 1.1).

Although ^{13}C NMR would allow the two metabolites to be distinguished, the coumarin was not isolated in large enough quantities to allow detection of all twelve of the carbon signals. An nOe experiment revealed no indicative correlations which would reliably identify the isomer present.

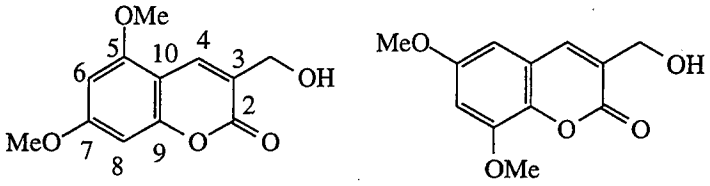

Figure 1.1 Two possible isomers of the phytotoxic coumarin, **1** and **2**.

A literature search revealed a recent paper from Ayer's group that included the isolation of a 3-hydroxymethyl-6,8-dimethoxycoumarin from the soil fungus, *Talaromyces flavus*.[5] An additional result of an nOe enhancement of the aromatic hydrogen at 6.48 ppm when the vinylic hydrogen at 7.70 ppm is presaturated indicates that these protons are peri to each other, thus suggesting the structure to be 3-hydroxymethyl-6,8-dimethoxycoumarin. The synthesis of 4-hydroxymethyl-5,7-dimethoxycoumarin was reported and the chemical shifts of this compound differ greatly from those of the isolated phytotoxin.[6] As all available spectroscopic data were identical to the reported data for the compound reported by Ayer, the phytotoxin produced by *Phyllosticta* was, in agreement with Ayer's analysis, proposed to be 3-hydroxymethyl-6,8-dimethoxycoumarin.

A crystallographic study would conclusively determine the correct isomer. Several attempts at crystallization were made, but due to the small quantities available and the lack of diffraction of the available crystals, this idea was eventually abandoned.

1.3 Summary

Coumarins are widely distributed among higher plants and are generally regarded as plant growth inhibitors with activity generally dependent upon the substitution pattern.[7,8] Coumarins are thought to inhibit the action of indole acetic acid, **3**, (IAA)(Figure 1.2). IAA is considered to be a primary phytohormone which induces elongation of coleoptile segments, as well as the the germination and growth of seeds, through its action as an auxin (plant growth promoter).

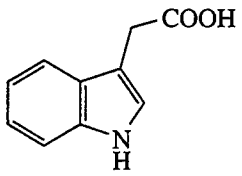

Figure 1.2 Indole acetic acid, **3**, a plant growth promoter.

It is well known that compounds produced by lower forms of plant life such as fungi and bryophytes have a pronounced effect on plant growth when administered exogenously and thus can be used to regulate the plants' development.[7,8] Coumarins have been previously reported to have phytotoxic activity.[5,7]

To improve crop viability, plant pathogens are often used to screen for resistant cultivars. The isolation and structural characterization of phytotoxins is of considerable agricultural interest because these compounds can be more readily used as available screening agents.[1] The phytotoxic secondary metabolites are useful

tools for screening plants for toxin insensitivity (disease resistance) as well as probes to study normal plant molecular biochemistry. A clear concept of the mechanisms of plant disease resistance could become an important tool for disease control in agriculture.

1.4 Experimental

General procedures. NMR spectra were recorded on a Varian XL-400 spectrometer. Chemical shifts were expressed by δ units in ppm from TMS as internal standard. IR spectra were recorded on a Mattson IR Spectrophotometer. MS were obtained from the mass spectrometry facility at University of Illinois, Urbana. CC adsorbents include Si gel (Aldrich) and Sephadex LH-20 (Pharmacia Fine chemicals, Uppsala, Sweden). The HPLC column employed was a Supelco C18 semiprep column, 5 μ pore, 10 mm x 25 cm using a Hewlett-Packard 1050 Series Pump and was monitored with an H-P 1050 Series Multiple Wavelength Detector at λ = 215 nm.

Culture Broth and Plant Assay. Cultures of *Phyllosticta sp.* were obtained from the mycological collection of the Department of Plant Pathology, Montana State University and were maintained on potato dextrose agar plates (Difco Laboratories, NJ). The fungus was innoculated on an autoclaved dry cornmeal/molasses media. The fermentation for toxin production was grown at room temperature for 30 days. The seeds of Kenaf, *Hibiscus sabdariffa var. altrissima* were

planted in plastic pots and grown in the laboratory. The plants used for assay during the purification procedure were 2-4 weeks old after germination. A 5 μL droplet of a 20 mg/mL solution of crude extract in 0.1% Triton X-100 in H_2O placed on a leaf over a puncture wound to enhance access to the leaf tissue. The leaves were placed on moist filter paper in a sealed Petri dish at room temperature for 48 h under light. The phytotoxic effects were observed as a 10 mm zone of necrosis, while negligible effects were observed with the 0.1% Triton X-100 solution as the control.

Extraction and Purification of 3-Hydroxy-6,8-Dimethoxycoumarin. The media was extracted with water and EtOAc successively and was then filtered *in vacuo*. The filtrate was then neutralized to pH 7.0 with 5 N NaOH and partitioned. The organic phase was combined and washed with brine. This EtOAc fraction was dried over anhydrous $MgSO_4$, filtered and then the solvent was removed *in vacuo* to produce the crude extract. The phytotoxic activity was found in the organic extract. First, the crude was partitioned into 2 mL fractions on a flash Si column with 1:1 hexane:EtOAc as the eluent. The active fractions, as determined by bioassay, were combined and further purified on a Sephadex LH-20 column with MeOH as the eluent. Final purification was accomplished with HPLC on a semiprep RP-C18 column using a gradient from 50% ACN:H2O to 100% ACN over 25 min while monitoring at λ=214 nm. Approximately 1.0 mg of the active substance was purified and the spectral data were identical to

the known coumarin. ^{1}H NMR ($CDCl_3$) δ: 2.40 t (1H, 1.6 Hz), 3.81 s (3H), 3.93 s (3H), 4.6 br d (2H, 1.6 Hz), 6.5 d (1H, 2.8 Hz), 6.7 d (1H, 3.1 Hz), 7.7 s (1H); ^{13}C NMR δ: 56.1 (OCH_3), 56.6 (OCH_3), 61.3 ($\underline{C}H_2OH$), 100.5 (C5 or C7), 103.0 (C5 or C7), 120.0, 129.0, 130.9, 131.0, 138.9 (C4), 152.6 (C2); nOe Correlations: δ 3.91-6.7 ppm; IR ν: 3400 (br), 3200, 1710, 1640, 1590 cm^{-1}. MS (EI^+) m/z 236 (100%), 218 (15), 207 (33), 191 (35), 190 (10), 177 (13), 165 (18), 148 (57); HRMS (EI^+), 236.0687 ($C_{12}H_{12}O_5$, Δ = 1.0 ppm).

1.5 References

1. Keen, In *Advances in Plant Pathology*, Ingram, Williams, Ed., Academic Press, **1982**, 1, 35-82.

2. Koshland, *Science*, **1990**, 248, 941.

3. Strobel, *Scientific American*, **1991**, 72-78.

4. Nishimura, Kohmoto, *Ann. Rev. Phytopath*, **1983**, 21, 87.

5. Ayer, Racok, *Can. J. Chem.*, **1990**, 68, 2085-2101.

6. Joshi, Usgaonkar, *Indian J. Chem.*, **1982**, 21B, 399-402.

7. Hallock, Clardy, Kenfield, Strobel, *Phytochemistry*, **1988**, 27, 3123-3125.

8. Goodwin, Mercer, *Introduction of Plant Biochemistry*, 2nd Ed., Pergamom Press, **1983**, pp. 569-580.

Chapter 2

Isolation and Structure of a Phytotoxin from *Alternaria crassa*

2.1 Introduction

Virtually all plants are susceptible to infection by several different pathogens that cause disease in the host plants by producing phytotoxins.[1] The known phytotoxins include a wide array of structures including terpenes, peptides, diketopiperazines, coumarins, polyketides, and spirocyclic lactams.[2,3,4,5] In the past, plant pathologists have utilized the secondary metabolites of pathogens of crop plants to screen the crops for disease resistant cultivars. The work in the previous chapter was motivated, in part, by just such an application. However, little work has been done on the pathogens that attack commercially unimportant plants. In particular, weed pathogens have been little studied. Examination of these pathogens could result in the discovery of novel bioactive and/or structurally diverse compounds.[2,3,4,5] Using the clues that nature has provided, one could take advantage of the phytotoxins produced by weed pathogens to provide a rich source of environmentally compatible

herbicides.[1] As one-third of all crop losses are due to weed problems, weed control is an important problem.[1]

Jimson weed, *Datura stramonium,* is considered a problem weed in some midwestern states and even in other countries.[6] This plant, also known as thornapple, is reported to infest fields of cotton, soybeans and other field crops. Common herbicides are relatively ineffective in controlling this noxious weed. For this reason, a search for one or more plant pathogens, that may serve as potential biological control agents, was undertaken.[6] Ultimately, *Alternaria crassa* was obtained from lesions in the leaves of Jimson weed which was infesting a field of soybeans near Southaven, Mississippi. The fungus was shown to be the causal agent of this severe leaf spotty disease.

An interesting attribute of many phytotoxins from fungi and bacteria is that they tend to have some degree of host-specificity, which allows for the development of potent, specific weed-killers.[6] These substances could also be of importance as a probe for the understanding of plant biochemistry. After extensive trials on a range of monocots and dicots, the host range of the pathogen was restricted to only a few members of the family Solanaceae, including a few tomato cultivars and Jimson weed, suggesting the possibility of a host-specific phytotoxin.[6] (Table 2.1)

Quite commonly in fungal infections involving chlorotic or necrotic leaf lesions, the causal organism produces one or more phytotoxins.[7,8,9] The phytotoxin, by itself, is capable of inducing some or all of the disease symptoms and is host-specific.[7,8,9] It is for this

Table 2.1 Host-specificity determined by the reaction of various plant species to *A. crassa*. R=resistant and S=susceptible to the pathogen.[6]

Family/species	Disease Reaction
Compositae	
Cocklebur	R
Sunflower	R
Convolvulaceae	
Morningglory	R
Cucurbitaceae	
Cantaloupe	R
Pumpkin	R
Graminae	
Corn	R
Johnsongrass	R
Rice	R
Sorghum	R
Wheat	R
Leguminosae	
Coffee senna	R
Soybean	R
Malvaceae	
Cotton	R
Velvetleaf	R
Solanaceae	
Eggplant	R
Bell Pepper	R
Tomato	S
Potato	R
Tobacco	R
Eastern Black nightside	R
Silverleaf nightshade	R
Jimsonweed	S

reason that *Alternaria crassa* was examined for its ability to make one or more phytotoxins.

2.2 Results and Discussion

Alternaria crassa was grown in Sabouraud Dextrose broth and the broth was eventually extracted into ethyl acetate. The purification of the active compound was guided by a leaf pucture wound assay. A droplet of a solution of the crude extract in 0.1% Triton X-100 in H_2O was placed on a leaf over a puncture wound of a Jimson weed leaf of to determine phytotoxicity.

The purification process eventually resulted in the isolation of a compound whose ^1H NMR contained two coupled doublets at 6.55 ppm and 6.91 ppm indicating the presence of a *para* substituted aromatic ring. The proton spectrum also showed two coupled methylene groups, one of which was definitely attached to a heterotatom. Mass spectrometry revealed a molecular weight of 138.1 corresponding to a molecular formula of $C_8H_{10}O_2$. The loss of a fragment with the mass of 18 indicated the loss of water. The IR spectrum corroborated the presence of an aromatic ring with the bands at 1410, 1465, and 1500 cm^{-1}. The IR spectrum also showed the appearance of at least one hydroxyl group. The structure of the active phytotoxin was deduced as para-hydroxyphenylethanol (PHPE), 4, from the combined spectral data.

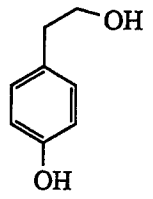

Figure 2.1 Para-hydroxyphenylethanol, **4.**

All of the spectroscopic data were consistent with para-hydroxyphenylethanol (Figure 2.1). Authentic PHPE possessed the identical spectral characteristics to those of the compound isolated from fungal cultures. This compound had previously been obtained in our laboratory from a culture of *Drechslera colocasiae* (pathogen of taro) by C. Hradil, J. Shumsky and S. Coval (unpublished results), and from *Phoma cypericola* a (pathogen of purple nutsedge) by A. Staley (unpublished results). This compound is also known from *Piricularia oryzae*, a pathogen of rice.[10]

The bioactivity of PHPE was tested on a range of plants using a standard leaf puncture assay method at 10, 5, and 2.5 μg/μL. At the highest concentration, after 48 hours of incubation, the compound caused a 1-6 mm nectrotic lesion in all plants tested including *Circium arvense, Manihot esculenta, Musa sp., Centaurea maculosa, Euphorbia milii,* and *Datura stramonium.* Lesser to no reactions were observed on leaves treated with 0.5 or 0.25 μg/μL of 4 in the test solution. This compound was therefore a non-host-specific phytotoxin that is less phytotoxic than the related compound, phenylethanol which is a

phytotoxin from *D. colocassiae* and studied comparatively with PHPE by S. Coval and G. Strobel (unpublished).

2.3 Summary

Based on these observations, it is apparent that *A. crassa* makes at least one phytotoxic substance. However, it is quite common for other members of this genus to make more than one phytotoxin.[7] Zinniol and its related family of compounds, the altusolenols, tenuazonic acid and derivatives thereof are commonly found as toxic products of *Alternaria sp.*[7,11,12] No evidence of a host specfic toxin was found in *A. crassa*; however, we have not ruled out the possibility that host-specific compounds could be produced by this fungus. Some fungi are known to produce some phytotoxins only in the presence of the host plant or host plant extracts.[13] The possibility that *A. crassa* could be capable of producing a host-specific phytotoxin under other fermentation conditions is an avenue that should be pursued.

The role of PHPE in symptom expression, and its mode of action need to be examined. Attempts to isolate PHPE from infected tissues and the isolation of the receptor/enzyme that is affected by the presence of the phytotoxin would lead to a greater understanding of the toxicity and possibly lead to the design of a more effective herbicide.

2.4 Experimental

General procedures. Nmr spectra were recorded on a Varian XL-400 spectrometer. Chemical shifts were expressed by δ units in ppm from TMS as internal standard. IR spectra were recorded on a Mattson IR Spectrophotometer. UV-Vis spectra were obtained from a Shimadzu UV160U UV-Vis Spectrophotometer. MS were obtained from the mass spectrometry facility at University of Illinois, Urbana. CC adsorbent was Sephadex LH-20 (Pharmacia Fine chemicals, Uppsala, Sweden). The HPLC column employed was a Supelco C18 semiprep column, 5 μ pore, 10 mm x 25 cm using a Hewlett-Packard 1050 Series Pump and was monitored with an H-P 1050 Series Multiple Wavelength Detector at λ = 215 nm.

Culture Broth and Plant Assay. Cultures of *Alternaria crassa* were obtained from the mycological collection of the Department of Plant Pathology, Montana State University and were maintained on potato dextrose agar plates (Difco Laboratories, NJ). The fungus was innoculated in 20 (500 mL) flasks with 250 mL of Sabouraud Dextrose Broth (Difco Laboratories, NJ) yielding 5 L of broth. The fermentation for toxin production was grown at 24°C and shaken at 200 rpm for 7 days. The seeds of Jimson weed, *Datura stramonium*, were planted in plastic pots and grown in the laboratory. The plants used for assay during the purification procedure were 2-4 weeks old after germination. A 5 μL droplet of a 20 mg/mL solution of crude extract in

0.1% Triton X-100 in H_2O placed on a leaf over a puncture wound to enhance access to the leaf tissue. The leaves were placed on moist filter paper in a sealed Petri dish at room temperature for 48 hr under light. The phytotoxic effects were observed as a 6 mm zone of necrosis, while negligible effects were observed with the 0.1% Triton X-100 solution as the control.

All other plant assays were run under standard leaf puncture wound assay conditions in the laboratory of Professor Gary Strobel, Department of Plant Pathology, Montana State University. The bioactivity of PHPE (Aldrich) was tested on a range of plants using a standard leaf puncture assay method at 10, 5, and 2.5 μg/μL. At the highest concentration, after 48 hours of incubation, the compound caused a 1-6 mm nectrotic lesion in all plants tested including *Circium arvense, Manihot esculenta, Musa sp., Centaurea maculosa, Euphorbia milii,* and *Datura stramonium.* Lesser to no reactions were observed on leaves treated with 0.5 or 0.25 μg/μL of 4 in the test solution.

Extraction and Purification of Para-hydroxyphenylethanol. The broth was filtered *in vacuo.* The filtrate was then neutralized to pH 7.0 with 5 N NaOH and extracted 2 times with 2.5 L of EtOAc. The organic phase was combined and washed with brine. This EtOAc fraction was dried over anhydrous $MgSO_4$, filtered and then the solvent was removed *in vacuo* to produce 200 mg of crude extract. The activity was found to be in the organic extract. The extract was further fractionated, guided by plant assay, with a modified Kupchan extraction. First, the

crude was partitioned between hexane and 90% MeOH:H_2O. The MeOH:H20 phase was diluted to 70% MeOH:H_2O and extracted with CH_2Cl_2. The MeOH:H_2O phase was again diluted to 50% MeOH:H_2O and extracted with EtOAc. The EtOAc fraction and the final MeOH:H_2O fraction were active in the bioassay and were combined to produce one fraction of 150 mg. The polar fraction was then loaded on a 50 g Sephadex LH-20 column using MeOH as the eluent and 4 mL fractions were collected. Active fractions, as determined by plant assay, were combined to give 55 mg. This column fraction was then purified by HPLC on a RP Supelco C18 semiprep column with a gradient of 50% MeOH:H_2O to 90% MeOH:H_2O over a period of 25 min, then eluted at 90% for 5 min before returning to 50% with a constant flow rate of 1.5 mL/min. The peak eluting at 11 min contained all activity. This fraction was then reinjected on the HPLC under the same conditions for further purification to yield 12.5 mg of pure compound, para-hydroxyphenylethanol. The spectral data was identical to the known compound. ^1H NMR ($CDCl_3$) δ: 2.60 t (2H), 3.55 t (2H), 6.55 d (2H), 6.91 d (2H), IR ν: 3400, 3200, 1500, 1465, 1410 cm^{-1}, UV λ_{max}: 280 nm, MS (EI) m/z 138 (22%), 107 (100), 91 (5), 77 (23).

2.5 References

1. Strobel, *Scientific American*, **1991**, 72-78.

2. Strobel, Kenfield, Bunkers, Sugawara, Clardy, *Experientia*, **1991**, 47, 821-826.

3. Kenfield, Bunkers, Wu, Strobel, Sugawara, Hallock, Clardy, *Experientia*, **1989**, 45, 900-902.

4. Hallock, Lu, Clardy, Strobel, Sugawara, Samsoedin, Yoshida, *J. Nat. Prod.*, **1993**, 56, 747-754.

5. Sugawara, Strobel, Fisher, Van Duyne, Clardy, *Proc. Natl. Acad. Sci., USA* **1985**, 82, 8291-8294.

6. Boyette, *Plant Science*, **1986**, 45, 223-228.

7. Nishimura, Kohmoto, *Ann. Rev. Phytopath*, **1983**, 21, 87.

8. Strobel, *Ann. Rev. Biochem.*, **1982**, 51, 309-333.

9. Wood, Franits, In *Phytotoxins in Plant Disease*, Ballio, Ed., Academic Press, **1972**, pp 530.

10. Deys, Bousquet, Barbier, *Phytopathol. Z.*, **1976**, 85, 176-178.

11. Stierle, Hershenhorn, Strobel, *Phytochemistry*, **1993**, 32, 1145-1149.

12. Stierle, Cardellina, Strobel, *J. Nat. Prod.*, **1989**, 52, 42-47.

13. Kenfield, Strobel, In *Host Plant Resisitance to Pests*, Hedin, ed., ACS Symposium Series, **1977**, 62, 35-46.

Chapter 3

Isolation and Structure of Syringolides, Elicitors from *Pseudomonas Syringae* pv. *Tomato*

3.1 Introduction

A major objective of plant pathology is to determine the molecular mechanism of disease resistance and plant recognition of pathogens.[1] When the plant is infected with a pathogen, a series of biochemical events occur as a part of a localized defense mechanism known as the hypersensitive response (HR).[1,2] The HR includes such events as rapid necrosis of host cells in the vicinity of the pathogen, an increase in the DNA transcription of the enzymes required in the production of phytoalexins, depolarization of the plant cell wall, and release of lytic enzymes from the plant cells. This active defense reaction results in the rapid localized plant cell death followed by accumulation of antimicrobial phytoalexins near the site of infection.[1]

Disease resistance in plants often results from an incompatibility between the host and the pathogen that is defined by specific genetic factors in both organisms. In this type of interaction, disease resistance is conferred by a dominant gene for resistance in the host and a corresponding dominant gene for avirulence in the pathogen.[1] Gene-

for-gene theory states that a specific plant receptor encoded by the plant resistance gene binds an elicitor resulting in an immune response in a fashion analagous to an antigen in mammalian systems. The dominant avirulence gene in the bacteria codes for an elicitor which is the protein product or a metabolite derived from the protein product's catalytic activity.

Although avirulence genes have been cloned from different bacterial pathogens whose gene products have been characterized, no plant resistance genes have yet been cloned or identified nor has such a plant receptor ever been isolated. In fact, little is known about how plant disease resistance genes recognize pathogens or the mechanism by which the hypersensitive response is actually triggered.[3]

The production of specific elicitors has been firmly associated with avirulence gene function in only a few cases.[2] In one of these cases, *Pseudomonas syringae* pv. *glycinea* , the causal agent of soybean blight, four avirulence genes have been molecularly characterized; avirulence genes A-D. This bacteria/host system was determined to be a gene-for-gene system, when the avirulence gene B was linked to *Rpg1* (resistance gene locus). This system was studied in order to understand the mechanism of race specificity and disease resistance.[4,5]

Pseudomonas syringae pv. *tomato* was chosen to study the genetic factors that elicit HR on the nonhost, soybean.[4] The pathogen, *Pseudomonas syringae* pv. *tomato* expressing the avirulence gene D (*avrD*), was shown to elicit the HR on soybean cultivars carrying the resistance gene, *Rpg4*.[4,5] *AvrD* gene was known to be found in both

Pseudomonas syringae pv. *tomato* and *Pseudomonas syringae* pv. *glycinea* allowing a comparison study of the genetic and biochemical factors that determine disease resistance.[6]

The *AvrD* gene product was isolated and shown to be a 34 kD protein composed of 311 amino acids, with significant homology (86%) between the *Pseudomonas syringae* pv. *tomato* and the *Pseudomonas syringae* pv. *glycinea* gene products.[4] While the *AvrD* gene from *Pseudomonas syringae* pv. *tomato* was capable of producing the HR, the *Pseudomonas syringae* pv. *glycinea* gene product does not show the avirulence phenotype.[5,6,7] It has been postulated that the *Pseudomonas syringae* pv. *glycinea AvrD* protein lacks stability due to minor mutations, thus rendering it incapable of producing the HR.[7]

In earlier examples of work in this area, the protein produced by the avirulence genes was the elicitor. However, the protein produced by the pathogen, *Psuedomonas syringae* pv. *tomato* elicited no HR from the soybean cultivars. When the avirulence gene D was cloned and expressed in gram negative bacteria, two low molecular weight metabolites were produced extracellularly and were found to account for the elicitor activity. The single protein gene product of *avrD* is postulated to be an enzyme responsible for the production of the metabolites that function as elicitors.[6,7] Interestingly, the *AvrD* protein produced by *P. syringae* does not produce significant amounts of the elicitors. It has been further postulated the changes in the enzyme produced by this were drastic enough to significantly reduce the catalytic activity, thus curtailing production of the elicitors.[7] The

final result being *Pseudomonas syringae* pv. *glycinea* is a successful pathogen on soybean, whereas the soybean cultivars are resistant to *Pseudomonas syringae* pv. *tomato*.

The discovery of nonproteinaceous low molecular weight elicitors is of considerable importance for several reasons. To date, neither the biochemical functions of avirulence genes nor the molecular mechanism by which a signal molecule elicits the hypersensitive response is known.[1,2] Further work in this area would allow a greater understanding of active plant defense responses and of race specificity.

This chapter will describe the isolation and structure elucidation of the structure of the bacterial signal molecules which elicit an active plant defense response. These molecules were obtained by the overexpression of the avirulence gene D from *Pseudomonas syringae* pv *tomato* in Gram negative bacteria.

3.2 Results and Discussion

Pseudomonas syringae pv. *tomato* or *Escherichia coli* carrying the plasmid containing the avirulence gene D were cultured in liquid M9 media while shaken for 21 hours at 28 °C. Each liter of broth was extracted three times successively with 500 mL of freshly distilled EtOAc, after the pH had been adjusted to 5.0, and then taken to dryness *in vacuo*. The crude yields averaged 55 mg/L from the *E. coli* broths and 25 mg/L from the *P. syringae* broths.

Bioactivity was followed by a soybean leaf infusion assay. After 24 hours, the leaves of soybean cultivars possessing the *Rpg4* disease resistance gene were scored for the appearance of necrosis indicating the hypersensitive response. The best separations were achieved with a normal phase silica column. Further purification was accomplished with HPLC on a silica column. The isolation procedure resulted in two active compounds, syringolides 1 and 2.

Spectroscopic data indicated that the purified elicitors were similar compounds. The IR and UV-Vis spectra were nearly identical, while the mass spectrum show a molecular weight difference of 28 mass units. ^{1}H NMR spectra differed only in integration of the methylene envelope protons and the ^{13}C NMR spectra of syringolide 2 showed the presence of two additional signals at 29 ppm. This evidence along with data accumulated in a ^{1}H-^{1}H COSY experiment shows syringolide 2 to contain two methylenes more than syringolide 1 in the corresponding hydrocarbon chain.

High resolution mass spectroscopy of syringolide 2 indicated a molecular formula of $C_{15}H_{24}O_6$. ^{1}H and ^{13}C NMR suggested the presence of a C_7H_{15} chain and a $C_8H_9O_6$ ring system containing two oxygenated methylenes, three oxygenated methines, a carbonyl, and two other oxygenated quaternary carbons. Since no double bonds appeared to be present and the molecular formula required four degrees of unsaturation, the molecule was assumed to have a tricyclic ring system.

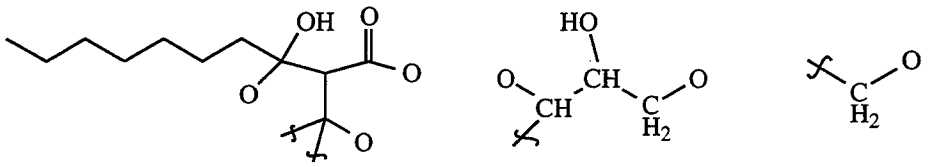

5 6 7

Figure 3.1 Partial structures of the plant elicitor.

The ring system contained two exchangeable protons indicating two hydroxyl groups, which were located by a secondary deuterium isotope shift experiment and acetylation. With the help of chemical shifts and INAPT, ^{1}H-^{1}H COSY and coupling experiments (Table 3.1), the connectivities of three partial structures, **5**, **6**, and **7** were established (Figure 3.1).

The partial structures of **5**, **6**, **7** complete the structure of syringolide 2, but there are many structures that could be reasonable derived from the combination of these fragments. However, the experimental $^{1}J_{C\text{-}H}$ values preclude the presence of any 3-membered rings. Also, the ^{13}C peak at 172 ppm was designated as a γ-lactone carbonyl due to the presence of an IR band at 1773 cm^{-1} and chemical shift. This additional information allowed the two structures, **8** and **9**, to be proposed. The availability of a simple biosynthetic pathway through condensation of a β-keto alkanoic acid and a 5-carbon keto-sugar greatly increases the plausibility of these structures.[8]

Table 3.1. NMR data for syringolide 2

Position	δ^1H	$\delta^{13}C$	INAPT correlations	^1H-^1H COSY
1	-	172.7 (s)		
2	3.08 (br s)	59.7 (d)	1, 3, 4, 1' ,2'	5.3
3	-	108.8 (s)		
4	1.87 (dd J=8.4)	39.4 (t)	2, 3, 6	1.5, 1.6
5a	1.48 (m)	24.4 (t)		1.3, 1.6, 1.9
5b	1.60 (m)			1.3, 1.5, 1.9
6	1.29 (m)	30.4 (t)		
7	1.29 (m)	29.9 (t)		
8	1.29 (m)	32.5 (t)		
9	1.29 (m)	23.3 (t)		
10	0.88 (t J=7)	14.3 (q)		1.3
1'a	4.30 (d J=10.3)	75.6 (t)	1, 2', 3', 4'	4.7
1'b	4.65 (d J=10.3)		1, 2, 3, 2', 3', 4'	4.3
2'	-	99.0 (s)		
3'	4.48 (br s)	92.2 (d)	1', 2', 4', 5'	3.9
4'	4.13 (dd J=4.1, 2.9)	75.4 (d)	1', 2', 3', 5'	3.8, 3.9, 4.27
5'a	3.81 (dd J=10, 2.9)	74.9 (t)	4'	3.9, 4.1
5'b	3.94 (dd J=10, 1.1)		2', 3', 4'	3.8, 4.1, 4.5
3-OH	5.31 (d J=1.8)		2, 3, 4	3.1, 4.1
4'-OH	4.27 (d J=4.1)			

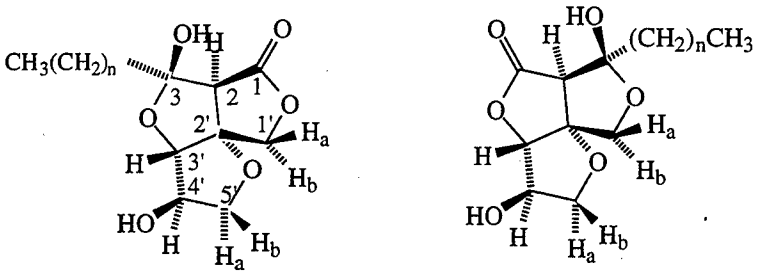

8 **9**

Figure 3.2 Two possible three-dimensional structures of syringolide 2, **8** and **9**.

The final structure of syringolide 2 was determined by X-ray crystallography (Figure 3.3).[8] After numerous crystallization attempts, suitable crystals were finally formed by vapor diffusion of hexanes into a concentrated solution of the elicitor in *n*-butyl acetate. Syringolide 2 crystallized as colorless plates with the dimension of 0.05 x 0.2 x 0.54 mm. The data was collected on a Siemens R3m diffractometer and the structure was solved by direct methods using SHELXTL with a final agreement factor of 0.051. There were no intramolecular hydrogen bonds in the crystal structure.

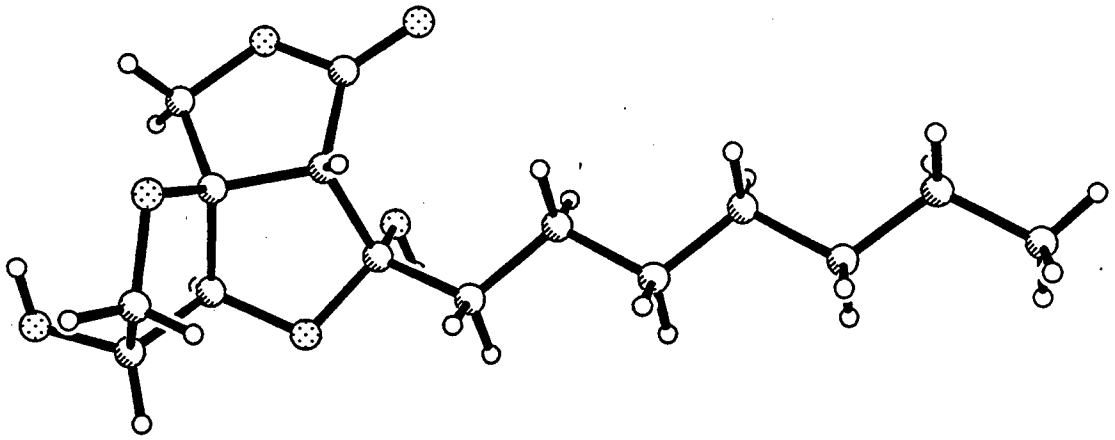

Figure 3.3 Computer generated drawing of the x-ray structure.

The relative stereochemistry of the syringolides was determined by X-ray crystallography and supports the proposed biosynthetic pathway (Figure 3.4). This pathway supposes the syringolides are derived from the condensation of xylulose and a β-keto acid.[8] While it is not uncommon to find acylated sugars as natural products, the combination of molecules from these two metabolic pathways via a carbon-carbon bond to make a C-glycosidic lipid, as in the syringolides, does not seem to have been observed before. However, compounds such as sphydrofuran and the butanolides are well known secondary metabolites which are examples of the condensation of 3-carbon ketones with either β-keto acids or 2-ketopentoses.[8]

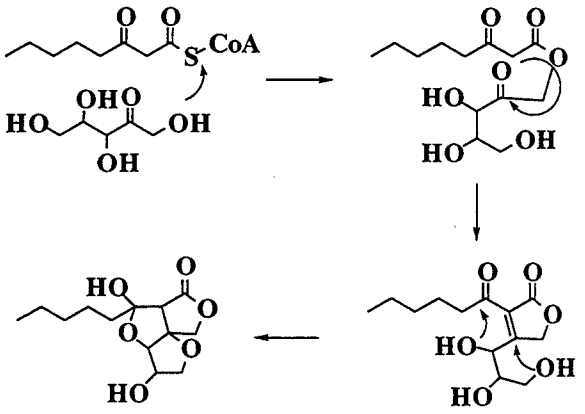

Figure 3.4 Possible biosynthetic pathway of the syringolides.[8]

The tricyclic ring system of the elicitors occurs as one of two possible enantiomers. As discussed before, only the relative stereochemistry has been defined by X-ray crystallography. Since *D*-xylulose is presumed to be the naturally occurring precursor, the

absolute stereochemistry is anticipated to be as depicted in Figure 3.5 (2S, 3R, 2'R, 3'S, 4'R).

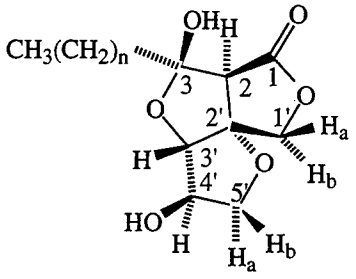

Figure 3.5 Final structure of the syringolides (n=4, syringolide 1; n=6, syringolide 2).

3.3 Summary

Two novel C-glycosidic molecules were isolated and characterized, syringolides 1 and 2, which are responsible for the elicitor activity of *Pseudomonas syringae* pv. *tomato* on the nonhost soybean cultivars. These molecules appear to be produced by avirulence gene D. This work represents the first evidence of nonproteinaceous low molecular weight natural products as elicitors of plant hypersensitivity.

The identification of the elicitor is the first step in the elucidation of the cell-signalling pathway of plant disease resistance. In the future, further studies with the receptor and the signal molecule could help elucidate the role the resistance gene plays in the mechanism of pathogen recognition and the defense response. The identification of a specific receptor would enable us to begin to probe

the molecular basis of the plant hypersensitive response. A clear concept of the mechanisms of plant disease resistance could become an important tool for disease control in agriculture.[1,9]

3.4 Experimental

General procedures. Mass spectra were determined using a Fissons VG autospec Q or a VG ZAB IFHF (high resolution) or a VG 7070 EHF instrument. UV spectra were recorded on a Perkin-Elmer 202. Infrared spectra were taken on a Nicolet FTIR or on a Perkin-Elmer Model 137. Optical rotations were obtained with a Perkin-Elmer Model 241 polarimeter with a 10 cm cell. NMR experiments were conducted using a GE-NMR QE300 or a Bruker 500 MHz instrument; chemical shifts are reported relative to Me_4Si. Carbon multiplicities were determined using APT or DEPT. One-bond C-H correlations were obtained using PSCSCM or HMQC optimized for 120 Hz and $^1J_{C-H}$ were measured by gated decoupling of ^{13}C spectra. Long-range C-H correlations were obtained by selective INEPT (INAPT) experiments and by HMBC and by CSCMLR, normally optimized at 10.7, and 6.25 Hz, respectively.

Soybean hypersensitive response determination. The elicitor activity of culture fluids, column fracions, etc. was determined by the soybean leaf bioassay. Generally, column fracions were dried, weighed, and redissolved at known concentrations in 95% ethanol. The

resultant solutions were bioassayed by infiltrating into leaves of several soybean cultivars. These were scored after 24 hr. for the appearance of necrosis only on leaves on cultivars carrying the *Rpg4* disease resistance gene.[8]

Purifications of syringolides 1 and 2. Erlenmeyer culture flasks (2L) with 1 L of medium were seeded relatively heavily with bacteria taken from fresh agar plates and the flasks were shaken for *ca.* 21 hr. at 28°C. The contents were then centrifuged for 5 minutes at 7500 g to remove bacterial cells. The supernatant fluids were decanted and the pH was adjusted from the ambient value of 6.6-7.1 to 5.0 with concentrated HCl. Each liter of fluid was extracted three times with 500 mL portions of freshly distilled EtOAc; the extracts were then taken to dryness *in vacuo* at 40°C. The crude yield from *E. coli* preparations averaged 55 mg/L of fluid and from *P. syringae,* about 25 mg/L.

The crude extract was further purified by vacuum liquid chomatography.[8] A 30 mL sintered glass filter funnel tightly packed with 4 cm of Kieselgel 60H (EM#7736) was used. Combined extracts (1 g, from about 18 L fluids) dissolved in 5 mL of $CHCl_3$ were loaded on the column after equilibration with $CHCl_3$, and successively eluted with 25 mL of $CHCl_3$, 50 mL of 60%EtOAc/$CHCl_3$, 50 mL of 100% EtOAc and 50 mL of 50%EtOAc/MeOH. Fraction 2 (60%EtOAc/$CHCl_3$) contained most of the crude elicitor activity (300 mg). This fraction was further purified by HPLC using isopropanol/ EtOAc/hexane (1.5:43.5:55) on a Dynamax silica gel column (1" x 25 cm). At 8

mL/min., syringolides 1 and 2 eluted with retention times of 51 and 44 min, respectively, and 6 and 5.5 mg of each was obtained per 50 mg injection. They were stored as waxy solids. Syringolide 2 was more readily crystallized than syringolide 1, and eventually crystals suitable for X-ray analysis were produced over several weeks vapor diffusion of hexane into a concentrated butyl acetate solution of syringolide 2.

Syringolide 1. Syringolide 1 was obtained in purified yield of about 1.8 mg per liter of culture fluids: mp 112.5-114.5°C; $[\alpha]^{24}_D$ = -83.66° (c=0.15, $CHCl_3$); UV(MeOH) λ_{max} 223 nm (ε=680), 245 (544), 315 (227); IR ($CHCl_3$) 3580, 2950, 2930, 2860, 1775, 1470, 1360, 1240, 1190, 1150, 1075, 1050, 980, 910 cm^{-1}; ^1H NMR (acetone-d_6, 300MHz), δ 0.88 (3H, t, J=8, H8), 1.3 (4H, br m, H6,7), 1.46 (1H, dtt, J=10.7, 6.7, 6.7, H5a), 1.6 (1H, dtt, J=10.7, 6.7, 6.7, H5b), 1.87 (2H, m, H4), 3.08 (1H, s, H2), 3.81 (1H, dd, J=10, 2.9, H5'a), 3.93 (1H, dd, J=10, 1.1, H5'b), 4.12 (1H, br t, J=4, H4'), 4.30 (1H, d, J=10.3, H1'a), 4.48 (1H, s, H3'), 4.65 (1H, d, J=10.3, H1'b), 4.30 (1H, br s, 4'OH), 5.34 (1H, d, J=1.8, 3-OH); ^{13}C NMR δ 14.3 (C8), 23.2 (C7), 24.0 (C5), 32.6 (C6), 39.4 (C4), 59.7 (C2), 74.9 (C5'), 75.4 (C4'), 75.6 (C1'), 92.2 (C3'), 99.0 (C2'), 108.8 (C3), 172.7 (C1); ^1H-^1H COSY correlations: δ 0.88-1.3; 1.5-1.3, 1.6, 1.9; 1.6-1.3, 1.5, 1.9; 1.9-1.5, 1.6; 3.1-5.3; 3.8-3.9, 4.1; 3.9-3.8, 4.5; 4.1-3.8, 3.9, 4.3; 4.3-4.1, 4.5, 4.7; 4.7-4.3; INAPT correlations: δ 3.1-39.4, 75.6, 99.9, 108.8, 172.7; 3.8-75.4; 3.9-75.4, 92.2, 99.0; 4.1-74.9, 75.6, 92.2, 99.0; 4.3-75.4, 92.2, 99.0, 172.7; 4.5-74.9, 75.4, 75.6, 99.0; 4.7-92.2, 172.7; 5.3-59.7, 108.8; MS (CI^+, NH_3) m/z 290 (12%), 272 (51), 264 (10), 256 (19), 255 (100), 254 (10), 239 (15), 236 (16), 230 (23), 229 (12), 228 (10), 212(12), 211

(47), 210 (10), 200 (18), 197 (10), 195 (13), 186 (20), 183 (12), 188 (10, 169 (16), 116 (13), 99 (13), 72 (11), 58 (19), 45 (14), 44 (25); HRMS (CI^+, NH_3), 269.1614 ($C_{13}H_{24}NO_6$=290.16036, Δ=3.6 ppm).

Syringolide 2. Syringolide 2 was obtained in purified yield of about 2 mg per liter of culture fluids: mp 123-124°C; $[\alpha]^{24}_D$ = -75.91° (c=0.22, $CHCl_3$); UV(MeOH) λ_{max} 220 nm (ε=355), 240 (255), 317 (248); IR ($CHCl_3$) 3583, 2956, 2930, 2873, 1773, 1466, 1377, 1244, 1186, 1152, 1074, 1047, 1026 cm^{-1}; MS (CI^+, CH_4) m/z 301 (9%), 283 (16), 241 (30), 239 (20), 223 (9), 211 (17), 197 (14), 145 (9), 127 (72), 85 (13), 69 (12), 61 (100). HRMS (CI^+, CH_4) 301.1638 ($C_{15}H_{25}O_6$, Δ=4.7 ppm); NMR data for syringolide 2 are given in Table 3.1.

Single crystal X-ray structure determination of syringolide 2. Syringolide 2 crystallized as colorless plates from n-butyl acetate/hexane, and a single crystal with dimensions 0.05 x 0.2 x. 0.55 mm was selected for analysis. All measurements were done on a Siemens R3m diffractometer using graphite monochromated CuKα radiation (λ=1.54180 Å). Preliminary diffraction photographs displayed monoclinic symmetry, and accurate lattice constants of a = 8.0720(10), b = 5.7850(10), c = 16.773(4) Å, β = 90.39(2)° were determined by a least-squares fit of 25 diffractometer-measured 2θ values in the range of 35-45°. Systematic extinctions, crystal density, and optical activity were uniquely consistent with space group $P2_1$ with one molecule of composition $C_{15}H_{24}O_6$ forming the asymmetric unit. A total of 1247

reflections with $2\theta \leq 116°$ were collected using a variable speed θ:2θ scan. No absorption or decomposition corrections were made. After correction for Lorentz, polarization, and background effects, 1173 of the 1247 unique reflections (94%) were judged observed ($|F_0| \geq 4\sigma|F_0|$). The structure was solved by direct methods and refined by full-matrix least-squares using SHELXTL. Anisotropic thermal parameters were employed for the nonhydrogen atoms and the hydrogen atoms rode on the heavy atoms with fixed geometry. The final agreement was R = 0.051.

3.5 References

1. Keen, *Annu. Rev. Genet.*, **1990**, 24, 447-463.

2. Thompson, Burdon, *Nature*, **1992**, 360, 121-125.

3. Kobayashi, Tamaki, Keen, *Proc. Natl. Acad. Sci. USA*, **1989**, 86, 157-161.

4. Kobayashi, Tamaki, Keen, *Mol. Plant-Microbe Interact.*, **1990**, 3, 94-102.

5. Keen, Buzzell, *Theor. Appl. Genet.*, **1991**, 81, 133-138.

6. Keen, Tamaki, Kobayashi, Gerhold, Stayton, Shen, Gold, Lorang, Thordal-Christensen, Dahlbeck, Staskwicz, *Mol. Plant-Microbe Interact.*, **1990**, 3, 112-121.

7. Kobayashi, Tamaki, Trollinger, Gold, Keen, *Mol. Plant-Microbe Interact.*, **1990**, 3, 103-111.

8. Midland, Keen, Sims, Midland, Stayton, Burton, Smith, Mazzola, Graham, Clardy, *J. Org. Chem.*, **1993**, 58, 2940-2945.

9. Moffat, *Science*, **1992**, 257, 482-483.

Chapter 4

Isolation and Structure of Insect Deterrents and Antifungals from Epiphylls

4.1 Introduction

Epiphylls are communities of leafy liverworts, mosses, lichens, bacteria, algae, and fungi growing on the surfaces of leaves.[1] The major structural component of these communities are the leafy liverworts of the families Lejeuneaceae, Frullaniaceae, and Radulaceae.[1,2] In rainforests of the neotropics, epiphylls thrive on a variety of understory plants with long-lived leaves. Epiphyll load varies among host species and is also dependent upon leaf age.[2]

Epiphylls may appear, upon first inspection, to be parasites reducing the fitness of the host plant by decreasing the leaves' light absorption, by injuring the leaf tissue or cuticle or by absorbing nutrients and water from the leaf.[2] However, evidence suggests the host plant may derive benefits from the epiphylls. These potential benefits may include a transfer of nutrients and water, protection from microbial plant pathogens and reduction in herbivory.[3,4]

In fact, recent studies suggest that epiphylls can reduce herbivore damage by the fungus-growing, leafcutter ant *Atta cephalotes*.[5] Since

leaf-cutting ants of the genera *Atta* and *Acromyrmex* are among the most destructive insect pests of crops in the neotropics and may represent 'key-stone' species in tropical ecosystems, this information could be of significant agricultural interest.[6] Leaf-cutter ants collect leaf material to feed their mutualistic fungus and, in this process, can defoliate entire trees in an evening. Thus, if an effective antifeedant could be developed to deter leafcutter ants from crop plants in Central and South America, the deterrent could be of widespread agricultural use.[6] The idea of this study was to determine if epiphylls produced a secondary metabolite which had antifeedant activity and to understand more of the feeding behavior of the insects with a long-term goal of reducing herbivory on crop plants.[5]

The original impetus for examining epiphylls for the production of compounds with ant deterrency came from the original work done by Mueller and Wolf-Mueller at La Selva Biological Station of the Organization for Tropical Studies, Puerto Viejo de Sarapiqui, Costa Rica.[5] The authors observed that leafcutter ants, *A. cephalotes*, tend to avoid leaves laden with epiphylls and undertook the study of the ecology of the system. These studies revealed that indeed the ants prefer to cut leaves free of epiphylls. However, it was not clear whether the ants' preference for leaves free of epiphylls was due to chemical protection of the leaves from a constituent of the epiphylls or whether it was due to physical protection preventing the foragers from cutting and shredding the leaves.[5] Because of the protective effect from herbivore damage, it would be of interest to determine if there is

a chemical deterrent and, if so, to isolate and characterize the compound(s) responsible for the activity.

As *Atta cephalotes* forage primarily to gather plant material for their mutualistic fungus, the selection of and exploitation of vegetation by the ants is a different issue from feeding and digestion, so the factors initiating foraging and the selection of plant material are not necessarily straightforward.[6,7,8,9] Our initial hypothesis was that liverworts produce antifungals as a natural competition process in the epiphyllous community and, incidently, deter foraging by leafcutter ants due to the effect of fungicidal constituents on their mutualistic fungus. This hypothesis was supported initially by previous work finding antifungals produced by liverworts[2,10] and later by the isolation of ant-deterrent compounds from angiosperm plants that tended to contain antifungal activity (Figure 4.1).[11,12,13]

Besides the ones already shown, several antifeedants and deterrents have been isolated and identified from numerous plant species in recent years (Figure 4.2).[14,15,16,17,18] This research is the first attempt to isolate antifeedant and antifungal metabolites from epiphylls.

10

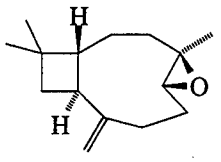

11

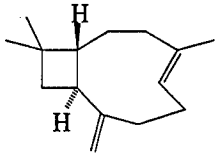

12

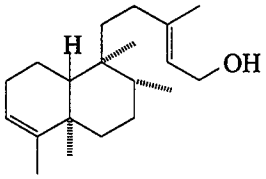

13

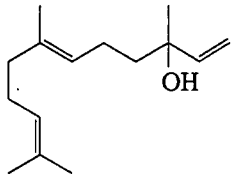

14

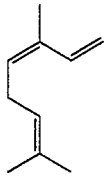

15

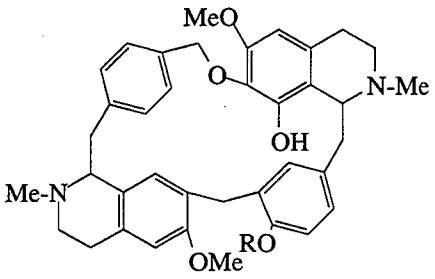

Figure 4.1 Antifeedants which are also antifungal, **10-15.**[11,12,13] (**10**, caryophyllene epoxide; **11**, caryophyllene; **12**, kolavenol; **13**, nerolidol; **14**, ocimene, **15**, cissampentin)

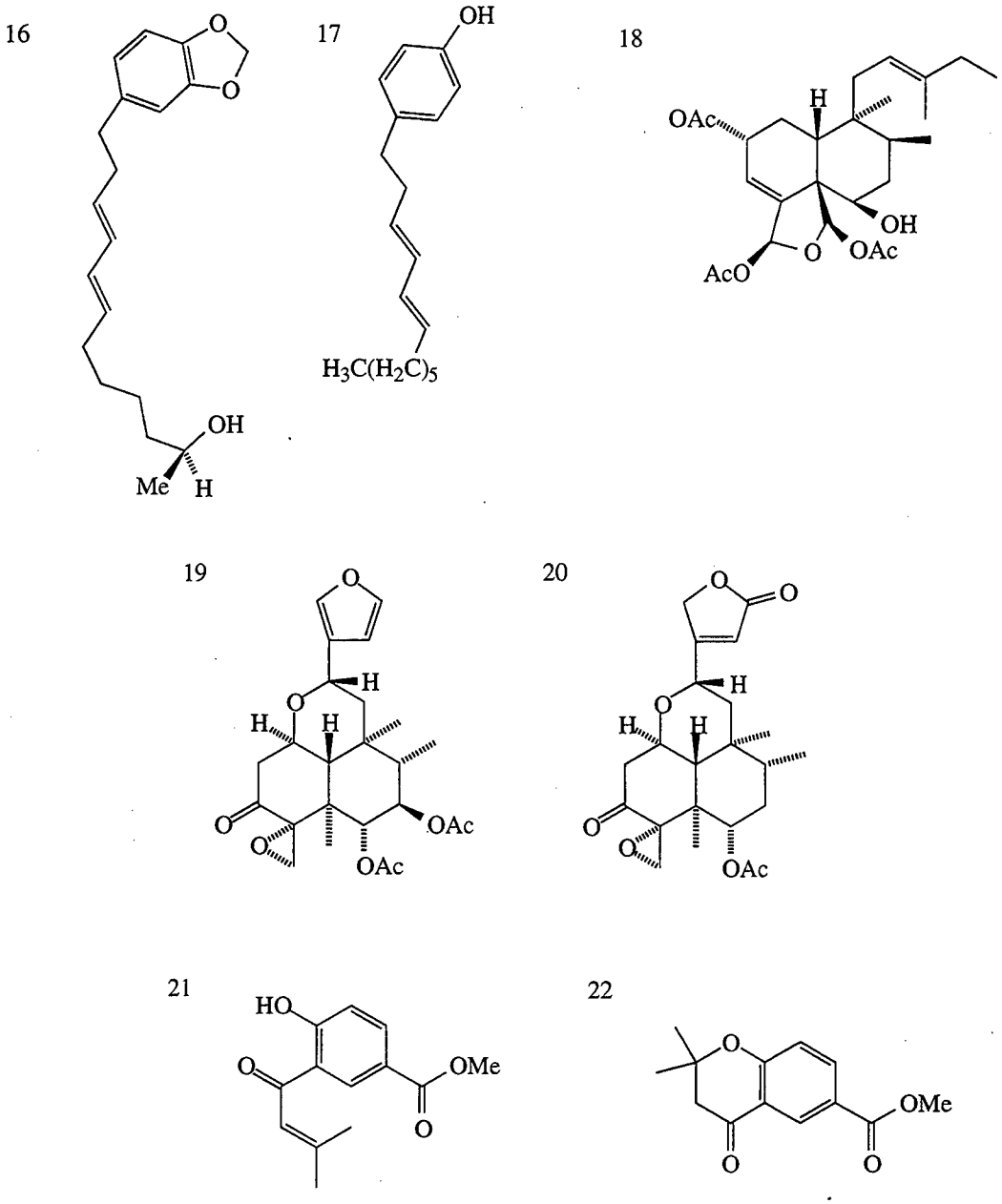

Figure 4.2 Known leafcutter ant deterrents, **16-23**.[14,15,16,17,18] (**16**, villiramulin A; **17**, villiramulin B; **18**, corymbotin; **19**, cornutin A; **20**, cornutin B; **21**, methyl taboganate; **21**, 2,2-dimethyl-6-carboxychoman-4-one)

4.2 Results and Discussion

Four colonies of leafcutter ants, *A. cephalotes*, with one queen each and their mutualistic fungus were collected at La Selva Biological Station of the Organization for Tropical Studies, Puerto Viejo de Sarapiqui, Costa Rica. At this time, epiphylls were also collected from the leaves of the native host plant, *Cyclanthus bipartitus*, growing in the understory of primary rainforest since leafcutter ants prefer to cut leaves from this plant species. The primary component of the epiphylls from the leaves of this plant at this site were liverworts of the family Lejeuneaceae. Field studies indicated that extracts from this liverwort alone accounted for a majority of the antifeedant activity.

The colonies were maintained at Cornell University and fed local plant leaves. In order to determine antifeedant activity, a bioassay was developed to rate the ants' preferences. Insect deterrent activity of extracts was tested with oat flakes laced with 10 μL of a test solution, dried for 0.5 hr to allow evaporation of the solvent. A flake with 10 μL of the solvent served as the control. The flakes were then presented to the ants in a foraging arena. In a given trial, all fractions of an extract and a control were presented to the ants simultaneously. Flakes were arranged in an array of two rows; the position of each flake in the array was randomized in each trial. The activity of fractions was tested in ten such trials by scoring the relative rate at which foragers picked up specific oat flakes, carried them toward their nest, and exited the foraging arena. A resulting value was determined from the order at

which specific flakes were taken, averaged over ten trials and served as a measure of relative deterrency.

In order to also test our hypothesis that the compound(s) produced by the liverwort would also be antifungal to the *A. cephalotes*' fungus, the fungus was cultured in our laboratory and an antifungal bioassay was developed.[19] *Atta cephalotes* cultivate a monoculture of a fungus of family Lepiotaceae.[20] The taxonomy of the fungus is still under debate, although it appears to be closely related to the free-living fungi of the genus *Leucoagaricus*. The fungus was cultured for 20 days in Potato Dextrose Broth with 0.5% Tryptone while shaking. In liquid culture, the fungus grows as clumps of mycelium, but hyphal tips separate from these clumps to float in suspension. 1.0 mL of this suspension was added to liquid media along with a solution the extract to be tested. All assays were run in triplicate. Cultures were shaken for 2 weeks, filtered, and the fungal biomass was weighed. Antifungal activity was defined as the reduction in biomass production relative to the control.

Initial fractionation with a modified Kupchan scheme resulted in four fractions of increasing polarity. As all of the antifungal and antifeedant activity was contained in the hexane fraction, this fraction was submitted to column chromatography for further purification. Separation on the Sephadex LH-20 column yielded three active fractions. One fraction contained antifeedant activity, one fraction contained antifungal activity and a third fraction contained both activities.

As the fraction with the antifeedant activity was the cleanest, its structure determination was undertaken first.

High resolution mass spectroscopy of the antifeedant indicated a molecular formula of $C_{15}H_{24}O_2$. ^1H and ^{13}C NMR suggested the presence of a ring system containing four methylenes, one downfield methine, two typical methines, a carbonyl, and three other quaternary carbons. Integration of the proton spectra and the DEPT spectra were consistent with one exchangeable proton. The main functional group appeared to be a 1,3 diketone. ^1H NMR shifts are similar to other enolone moieties in ring systems.[21] Also, the ^{13}C peak at 171.6 ppm was designated as the two carbons of the enolone system due to chemical shift. The presence of an enolone was also supported by the three IR bands at 1705, 1688, and 1645 cm^{-1}. Although the decoalesced shifts of an enolone are typically in the range of δ 190 and 150 ppm, the coalesced peaks are present as the average of these two peaks because proton exchange is faster than the NMR time scale.[21] Low-temperature NMR experiments were performed on this sample and no change was observed. However, it is not unusual for the proton exchange to be seen even at -60°C.[21] The enol form is highly favored in nonpolar solvents and the presence of an enol hydroxyl supported by the a signal in the NMR at about δ 14 ppm and a diffuse band in the IR at 3021 cm^{-1} indicating a trans-enol involved in an intermolecular hydrogen bond.

The molecular formula required four degrees of unsaturation. Including the presence of an enolone system, the molecule was assumed to have a bicyclic ring system. With the help of chemical

shifts, HMQC, ^{1}H-^{1}H COSY, DEPT, and coupling experiments (Table 4.1), partial structures were established. There are many structures that could be reasonably derived from the combination of these fragments. However, the experimental $^{1}J_{C-H}$ values preclude the presence of any 3-membered rings. Also, the use of HMBC experiments helped to establish the connectivities of the partial structures. This additional information allowed the structure to be proposed (Figure 4.3).

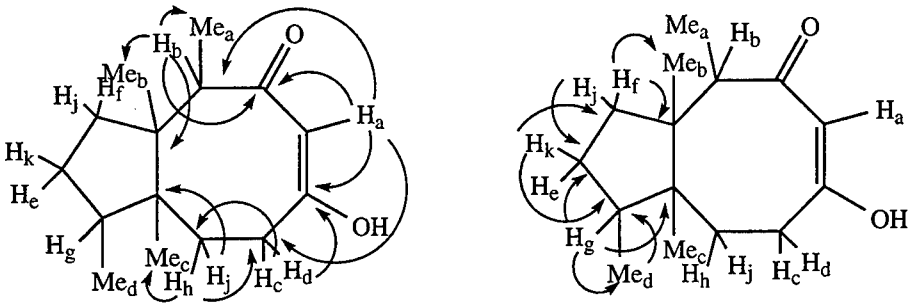

Figure 4.3 HMBC correlations used to determine the structure of **23**.

The relative stereochemistry depicted was determined with a ROESY experiment. The correlation between the two ring junction methyls and another correlation between the other two methyls indicated a cis ring junction (Figure 4.4). Confirmation of this structure could be rigorously determined by X-ray crystallography and the attempt to grow crystals is being made.

Table 4.1. NMR data for **23**

Position	δ^1H	δ^{13}C	DQ-COSY	HMBC correlations
Me_d	0.92 (d, 3H)	19.1 (q)	$Me_{b,c}$ (weak)	44.5, 43.3, 30.5
Me_c	0.95 (s, 3H)	19.6 (q)		43.3, 47.6, 30.1*
Me_b	0.96 (s, 3H)	22.6 (q)		43.3, 47.6, 30.1*
Me_a	1.13 (d, 3H)	16.5 (q)		171.6, 40.7, 47.6
j	1.32 (m, 2H)	39.4 (t)		47.6, 44.5, 43.3, 30.5, Me_b
k		30.5 (t)		44.5, 39.4, Me_d
h,i	1.48 (m, 2H)	38.3 (t)	$Me_{b,c}$	171.6, 47.6, 44.5, 43.3, 30.1, Me_c
f	1.72 (dq, 2H)	39.4 (t)	j,$Me_{b,c}$	47.6, 40.7, 38.3, 30.5, Me_b
g		44.5 (d)	Me_d	47.6, 43.3, 38.3, 30.5, Me_d
e	1.85 (m, 1H)	30.5 (t)	f,g,j,k	47.6, 44.4(weak), 43.3, 39.4, Me_d
d	2.12 (dt, 1H)	30.1 (t)	c,h,i	171.6, 113, 43.3, 40.7, 38.3
c	2.52 (m, 1H)	30.1 (t)	d,h,i	171.6, 113, 43.3, 38.3
b	3.65 (q, 1H)	40.7 (d)	Me_a,d(weak)	171.6, 113, 47.6, 43.3, 39.4, 30.1, Me_a, Me_b(weak)
a	5.68 (s, 1H)	113.0 (d)	b,c,d	171.6, 40.7, 30.1, Me_a
l		43.3 (s)		
m		47.6 (s)		
n		171.6 (s)		

*The HMBC correlations from and the COSY correlations to Me_b and Me_c could not be distinguished.

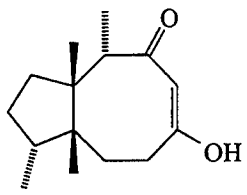

Figure 4.4 Structure of antifeedant isolated from epiphylls, **23**.

4.3 Summary

While 8:5 ring systems are uncommon in nature, there are a number of examples of these moieties in terpenoid natural products from algae, liverworts and fungi.[22,23,24,25,26] However, an extensive literature search has revealed no matches for the proposed structure, **23**, indicating a novel compound.

Currently, work is being done on the isolation of the other two active components of the epiphyll extract. There is very little of both of these compounds and they both appear to be small, lipophilic substances. The isolation and structure elucidation of all three components would complete an interesting ecological study and could contribute to the goal of controlling herbivory damage from leafcutter ants on the agricultural crops of Central and South America.

4.4 Experimental

General procedures. NMR spectra were recorded on a Varian XL-400 or a Varian XL-500 spectrometer. Chemical shifts were expressed by δ units in ppm from TMS. IR spectra were recorded on a Mattson IR Spectrophotometer. UV-Vis spectra were obtained from a Shimadzu UV160U UV-Vis Spectrophotometer. MS were obtained from the mass spectrometry facility at University of Illinois, Urbana. CC adsorbent was Sephadex LH-20 (Pharmacia Fine chemicals, Uppsala, Sweden). The HPLC column employed was a Hamilton RPLC-PRP semiprep column, 5 μ pore, 10 mm x 25 cm using a Hewlett-Packard 1050 Series Pump and was monitored with an H-P 1050 Series Multiple Wavelength Detector at λ = 215 nm.

Antifungal Bioassay. Fungus isolated from a laboratory colony of the leafcutter ant, *Atta cephalotes* (collected Jan. 1991 at La Selva, Costa Rica). The fungus was cultured for 20 days in Potato Dextrose Broth with 0.5% Tryptone (Difco) while shaking at 60 rpm. In liquid culture, the fungus grows as clumps of mycelium, but hyphal tips separate from these clumps to float in suspension. 1.0 mL of this suspension was added to 25 mL of liquid media in 125 mL flasks. Crude extract was dissolved in ethanol and 0.5 mL of the test solution was added to the innoculated flask. All assays were run in triplicate. The addition of 0.5 mL of ethanol served as the control. Cultures were shaken for 2 weeks, filtered, and the fungal biomass was weighed.

Antifungal activity was defined as the reduction in biomass production relative to the control.

Antifeedant Bioassay. Insect deterrent activity of extracts was tested in a laboratory colony of the leafcutter ant, *A. cephalotes* (collected Jan. 1991 at La Selva, Costa Rica). Oat flakes were laced with 0.02 mg of a test extract in 10 µL of ethanol or THF and dried for 0.5 hr to allow evaporation of the solvent. A flake with 10 µL of the solvent served as the control. The flakes were then presented to the ants in a foraging arena. In a given trial, all fractions of an extract and a control were presented to the ants simultaneously. Flakes were arranged in an array of two rows; the position of each flake in the array was randomized in each trial. The activity of fractions was tested in ten such trials by scoring the relative rate at which foragers picked up oat flakes, carried them toward their nest, and exited the foraging arena. Flakes that were picked up, but then dropped, were not scored. Flakes picked up first received the highest score, those picked up last received the lowest posible score of 1. The expected score for a flake with neutral activity (10*[n+1]/2) was then subtracted from the sum of all scores received by a fraction over the ten trials. The resulting value served as a measure of the relative deterrency.

Purification of 23. Initial fractionation with a modified Kupchan scheme resulted in four fractions of increasing polarity. First, the crude was partitioned between hexane and 90% MeOH:$H_2$0. The MeOH:H20

phase was diluted to 70% MeOH:H_2O and extracted with CH_2Cl_2. The MeOH:H_20 phase was again diluted to 50% MeOH:H_20 and extracted with EtOAc. As all of the antifungal and antifeedant activity was contained in the hexane fraction, this fraction was submitted to column chromatography for further purification. Separation on a 50 g Sephadex LH-20 column with 1:1 CH_2Cl_2 and MeOH as the eluent yielded a pure fraction containing only antifeedant activity. UV(MeOH) λ_{max} 233 nm (ε=3622), 310 (479); IR ($CHCl_3$) 3258 br, 2968, 2874, 1704, 1688, 1639 cm^{-1}; ^1H NMR ($CDCl_3$, 400MHz), δ 0.92 (d, 3H), 0.95 (s, 3H), 0.96 (s, 3H), 1.13 (d, 3H), 1.32 (m, 2H), 1.48 (m, 1H), 1.72 (dq, 2H), 1.85 (m, 1H), 2.12 (dt, 1H), 2.52 (m, 1H), 3.65 (q, 1H), 5.68 (s, 1H); ^{13}C NMR ($CDCl_3$) δ 16.5 (q), 19.08 (q), 19.6 (q), 22.6 (q), 30.1 (t), 30.6 (t), 38.3 (t), 39.4 (t), 40.7 (d), 43.3 (s), 44.5 (d), 47.6 (s), 113 (d), 171.6 (s); ^1H-^1H COSY correlations: δ 0.92-1.73; 0.955-1.13, 1.48, 1.7; 1.13-3.65; 1.3-1.7; 1.32-1.72; 1.48-2.12, 2.52; 5.68-3.65, 2.52, 2.12 HMQC correlations: δ .92-19.1, 0.95-19.6, 0.96-22.6, 1.13-16.5, 1.3-39.4, 1.32-30.5, 1.48-38.3, 1.7-39.4, 1.72-44.5, 1.85-30.5, 2.12-30.1, 2.52-30.1, 3.65-40.7, 5.68-113; HMBC correlations: δ 0.92-30.5, 43.3, 44.5; 0.955-30.1, 43.3, 47.6; 1.13-40.7, 47.6, 171.6; 1.30-22.6, 30.5, 43.3, 44.5, 47.6, 1.32-19.1, 39.4, 44.5; 1.48-0.95, 30.1, 43.3, 44.5, 47.6, 171.6; 1.7- 22.6, 30.5, 38.3, 40.7, 47.6; 1.72-0.92, 30.5, 38.3, 43.3, 47.6; 1.85-0.92, 39.4, 43.3, 44.5, 47.6; 2.12-38.3, 43.3, 113, 171.6; 3.65-0.96, 1.13, 30.1, 39.4, 43.3, 47.6, 113, 171.6; 5.68-1.13, 30.1, 40.7, 171.6; MS (EI^+) m/z 236 (25%), 221 (35), 203 (5), 161 (10), 137 (25), 123 (100), 109 (80); HRMS (EI^+), ($C_{15}H_{24}O_2$ = 236.177743, Δ= 0.5 ppm).

4.5 References

1. Berrie, Eze, *Annals of Botany*, **1975**, 39, 955-963.

2. Bien, *Substrate Specificity of Leafy Liverworts in a Costa Rican Rainforest*, Thesis, State University of New York at Stony Brook, **1982**.

3. Bentley, Carpenter, *Microb. Ecol.*, **1980**, 6, 109-113.

4. Bentley, Carpenter, *Oecologia*, **1984**, 63, 52-56.

5. Mueller, Wolf-Mueller, *Oecologia*, **1991**, 86, 36-39.

6. Cherret, Seaforth, *Bull. Ent. Res.*, **1968**, 59, 615-625.

7. Martin, *Invertebrate-Microbial Interactions*, Cornell University Press, **1987**, Chapter 6, pp 91-124.

8. Weber, *Science*, **1966**, **152**, 187-604.

9. Cherret, Powell, Stradling, In *Insect-Fungus Interactions*, Wilding, Ed., Academic Press, 1989, pp 92-120.

10. Lawrey, *The Bryologist*, **1986**, 89, 111-122.

11. Hubbell, Wiemer, Adejare, *Oecologia*, **1983**, 60, 321-327.

12. Howard, Cazin, Wiemer, *J. Chem. Ecol.*, **1988**, 14, 59-69.

13. Galinis, Wiemer, Cazin, *Tetrahedron*, **1993**, 49, 1337-1342.

14. Howard, Green, Wiemer, *J. Chem. Ecol.*, **1989**, 15, 2279-2288.

15. Roussis, Ampofo, Wiemer, *Phytochemistry*, **1990**, 29, 1787-1788.

16. Chen, Wiemer, *J. Nat. Prod.*, **1991**, 54, 1612-1618.

17. Chen, Galinis, Wiemer, *J. Org. Chem.*, **1992**, 57, 862-866.

18. Galinis, Wiemer, *J. Org. Chem.*, **1993**, 58, 7804-7807.

19. Cazin, Wiemer, Howard, *Appl. Env. Microbiol.*, **1989**, 55, 1346-1350.

20. Hervey, Rogerson, Leong, *Brittonia*, **1977**, 29, 226-236.

21. Floris, In *Chemistry of Enols*, Rappoport, Ed., John Wiley and Sons, **1990**, pp 147-306.

22. Strobel, Kenfield, Bunkers, Sugawara, Clardy, *Experientia*, **1991**, 47, 819-826.

23. Herout, In *Bryophytes: Their Chemistry and Chemical Taxonomy*, Zinsmeister, and Mues, Ed., Oxford Science Publications, **1990**, pp 83-102.

24. Schmitz, Hollenbeak, Vanderah, *Tetrahedron*, **1978**, 34, 2719.

25. Fenical, Schulte, Finer, Clardy, *J. Org. Chem.*, **1978**, 43, 3628.

26. Enoki, Furaski, Suehiro, Ishida, Matsumoto, *Tetrahedron Lett.*, **1983**, 24, 4341.

Chapter 5

Isolation and Structure of *Ras* Farnesylation Inhibitors from *Verticillum tenerum*

5.1 Introduction

The serendipitous discovery of a *ras* farnesylation inhibitor from extracts of *Verticillium tenerum* is a compelling example of how collaborative, interdisciplinary efforts can lead to exciting developments using biorational arguments. Biorationale involves using the understanding of the interactions of an ecosystem to determine sources of potentially bioactive chemicals. *V. tenerum* , the anomorphic form of a locally-occurring soil fungi, *Nectria inverta*, was collected along with some 200 other mycological samples from a primary forest in the Ithaca area by researchers at the Boyce Thompson Institute for Plant Research, who were seeking biocontrol agents for Japanese beetle larvae. Following the biorational arguments set forth by Eisner which state that different species of common soil fungi must compete for the same ecological niche, and could therefore produce effective antifungal agents,[1] a collaboration was established with the Boyce Thompson Institute to test the hypothesis using their fungal library and with Schering-Plough Corporation to run the bioassays.

Although not very promising as an antifungal agent, *V. tenerum* displayed cytotoxic and antibacterial activity. When submitted for a further battery of bioassays at Schering-Plough Corporation, this sample was found to inhibit the *ras* farnesylation enzyme, indicating a constituent natural product could be useful as an anti-cancer drug.

While many details remain unclear, there is little doubt that a mutated *ras* protein is involved in some forms of cancer. In fact, oncogenic *ras* is purported to be involved in 30% of human cancer cases, most notably in most cases of human colon and pancreatic carcinomas.[2] Not only is *ras* important in cell proliferation and thus in the development of cancer, it is also a primary link in signal transmission in the cell. For these reasons, the study of the mechanism of activation and of the oncogenesis of *ras* is of significant use in the study of cancer as well as understanding cell biochemistry. *Ras* genes code for a family of monomeric 21 kD proteins often referred to as *ras* p21. These guanine nucleotide binding proteins are found on the inner surface of the plasma membrane.[3] The *ras* protein is a type of G-protein that cells produce to regulate cell proliferation. Like other G-proteins, the *ras* protein binds GDP molecules in its resting or inactive state, but when activated, a GDP-GTP exchange occurs.[4] GTP binding induces a conformational change that allows the protein to participate in a growth promoting signal transduction pathway. *Ras*-GTP has only recently been discovered to direct the localization of the *raf* protein to the plasma membrane. Activated *raf* regulates a mitogen

activated protein (MAP) kinase cascade which eventually leads to transmittance of the proliferative signal to the nucleus.[5,6] With this mechanism, the *ras* protein is the common relay point for signals from all the growth factor receptors known so far.[7] The *ras* oncogene is almost identical with the normal *ras* gene, but its gene product has two critical amino acid substitutions that interfere with the shut-off mechanism. These mutations lock *ras* in the permanently 'on' position and can ultimately cause uncontrolled cell proliferation leading to the development of cancer.[4]

A recent discovery indicates the *ras* protein must undergo post-translational modification which is required for the protein to be directed to its position on the cellular membrane.[8,9,10,11,12] This modification involves, among other things, prenylation of the protein; the addition of a 15-carbon isoprenoid chain.[8,9,10,11] The attached prenyl group acts as a molecular anchor that allows the *ras* to attach to the plasma membrane.[13] Prenylation is an essential step in the production of a functioning *ras* protein. If the post-translational modification can be interrupted, the cancer cell growth could be controlled. Pharmacologists believe that this step might be a promising therapeutic target for chemotherapy[14,15] and a few years ago the enzyme, *ras* farnesyl transferase, was isolated.[8,10] Many proteins undergo prenylation, so there was originally much skepticism that this would be a specific target for inhibition. More recent work has revealed that while most proteins are prenylated with a 20-carbon geranylgeranyl group, the *ras* protein is modified by the attachment of

a 15-carbon farnesyl group (Figure 5.1).[8,13] The isolation of *ras* farnesyl transferase proved the notion that a different enzyme is involved in the addition of the geranylgeranyl group than in the addition of the farnesyl group. In fact, the attachment of a geranylgeranyl moiety to the *ras* p21 protein alters the final destination of the recently translated protein and, thus, its growth promoting function. This knowledge allows for the possibility of a selective inhibition of the farnesyl transferase without affecting prenylation of other proteins.

The two transferase enzymes are composed of the same alpha subunit, but have different beta subunits.[2] Therefore, a drug that could inhibit the beta subunit would be a promising lead for the controlling the development of cancer. One key to the type of prenylation a protein will undergo lies in the last four amino acids from the C-terminus, called the CAAX box.[2,8,9,10] The CAAX box consists of a cysteine, followed by two aliphatic amino acids, and ending in any of several different amino acids (X). If X=serine, methionine, or glutamine, the protein will be farnesylated. But if the final amino acid of the CAAX box is leucine or phenylalanine, then the isoprenoid used will be a geranylgeranyl group. Geranylgeranyl addition can also be achieved with two alternate motifs, a CC or CXC sequence on the end of the protein. The specificity of the transferase enzymes for the recognition of the CAAX box is quite high; encouraging hopes that farnesylation alone could be inhibited.[2]

The *ras* protein undergoes further processing steps before becoming a functioning protein in the cell membrane (Figure 5.1).[2,12]

Once the protein has been farnesylated, proteolysis of the AAX fragment occurs.[14] Recent experiments suggest that this step is essential for proper protein function since the association of *ras* p21 with particular cell fractions is dependent upon proteolysis. The third processing step common to *ras* proteins is the conversion of the C-terminal cysteine carboxylic acid into its methyl ester.[12] Such esterification is observed only on peptides prenylated on the C-terminal cysteine, with the presence of a farnesyl group being the most effective. Thus, specific isoprenoids might comprise effective recognition sites that direct the activity of the C-terminal protease and methyltransferase.[2,12,14]

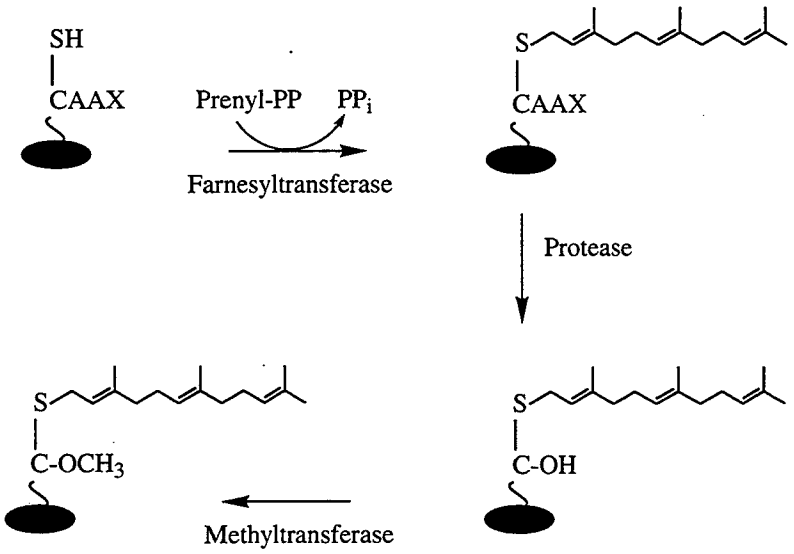

Figure 5.1 Post-translational modification of the *ras* p21 protein.

Although protein targeting is still poorly understood, it is clear that for the *ras* protein to be capable of its growth-promoting activity it must be directed to the correct location on the correct membrane.[13] While all the C-terminal modifications are important for directing the *ras* protein to its site on the cell membrane, other factors may also be required for membrane localization. In fact, it appears that post-translational modifications only direct *ras* p21 to the particular site of attachment on the membrane.[2,13,14] It is known that a series of six lysine residues just adjacent to the CAAX box are essential to lead the protein to the plasma membrane. This information has led to the recent speculation that the lysine-rich region helps the *ras* protein reach the correct membrane through interactions with specific protein molecules such as receptor or docking proteins.[2,14]

The identification and characterization of enzymes that are involved in the post-translation modification and membrane localization of the *ras* protein has provided a starting point for the development of potential inhibitors. This search for anti-*ras* drugs has focused on attempting to inhibit the farnesylation step for several reasons. Farnesyl transferase has been targeted primarily because studies have shown that isoprenoid modification alone is sufficient for oncogenic *ras* function, whereas carboxymethylation and proteolyis, while important, are not essential for membrane association or growth-promoting activity.[2] Also, it is known that the specificity of farnesyl transferase allows for selective inhibition without affecting prenylation of other proteins.

While the previous arguments focus on chemical specificity of possible inhibitors, new studies suggest that an inhibitor of *ras* post-translational modification may result in a biologically selective inhibition of the ras mitogenic pathway. Forms of oncogenic ras with impaired GTPase activity and genetically lacking the cysteine residue of the CAAX box have been found to inhibit membrane-bound *ras* function. However, forms of *ras* containing the GTPase activity yet still lacking the farnesylation site do not affect the membrane-bound ras function. Thus, only oncogenic *ras* would biologically inhibit the the *ras* pathway. These results suggest that if farnesylation is chemically inhibited, not only would there be less functional *ras* in the membrane, but the accumulation of nonfarnesylated oncogenic *ras* in the tumor cells would also selectively inhibit the growth-promoting activity of the functioning *ras*. However, since normal nonfarnesylated *ras* does not inhibit functioning *ras*, this effect would only be present in the tumor cells. Thus, for several reasons, pharmacologic inhibitors of *ras* farnesylation are likely to be very effective for blocking oncogenic *ras* function in tumors.[14]

The observation that *ras* farnesyl transferase did not require the entire intact ras p21 protein for farnesylation activity led to the attempt to use short peptides or peptide analogs as possible inhibitors. Initial studies revealed most tetrapeptides with the Cys-AAX sequence are competitive inhibitors of farnesyl transferase.[8,9,16] In fact, these smaller peptides have a higher affinity for the enzyme than the natural substrate.[16] The CAAX tetrapeptide was the minimal sequence

required for interaction with the farnesyl transferase and was, thus, the starting point for developing peptide inhibitors.[16]

Several peptides and peptide analogs have been studied.[8,9,15,16,17,18] So far the most interesting of these are the benzodiazepine peptidomimetics from Genentech[18] and a set of tetrapeptide analogs from Merck.[17] The benzodiazepine derivatives took advantage of the knowledge that peptides like CVFM (Cys-Val-Phe-Met) that contain a charged amino terminus and an aromatic group in the third position of the CAAX sequence inhibit the transferase enzyme without becoming farnesylated. However, as such tetrapeptides are ineffective when added to intact cells due to bioavailability, peptidomimetic analogs were developed that maintained the dipeptide turn and the amino and carboxy terminal

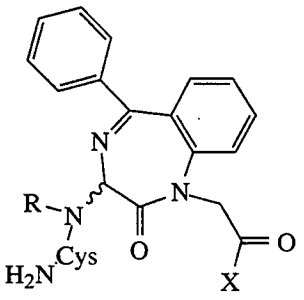

Figure 5.2 Benzodiazepine Analogs, **24**. (BZA-1, R=H, X=MetCOOH; BZA-2, R=CH_3, X=MetCOOH; BZA-3, R=CH_3, X=SerCOOH; BZA-4, R=CH_3, X=LeuCOOH; BZA-5, R=CH_3, X=MetCOOMe; BZA-6, R=CH_3, X=$MetCONH_2$).

interactions (Figure 5.2). Assays indicate the benzodiazepine analogs are capable of selectively inhibiting farnesyltransferase *in vitro*.[18]

Another set of peptide analogs used the carboxy terminus of the human K4A-Ras, CIIM, as a template to develope the analogs, *N*-{2(S)-{2(R)-amino-3-mercaptopropylamino}-3(S)-methyl-pentyl}isoleucyl-homoserine lactone and *N*-{2(S)-{2(R)-amino-3-mercaptopropylamino}-3(S)-methyl-pentyl}isoleucyl-homoserine (Figure 5.3). Due to increased bioavailability, these inhibitors are better drug candidates than the tetrapeptides and, more importantly, these inhibitors selectively target *ras* transformed cells without affecting the viability of normal cells.[15,18] Currently, Merck is using the lactone analog as a prototype for ras farnesyl transferase inhibitors.

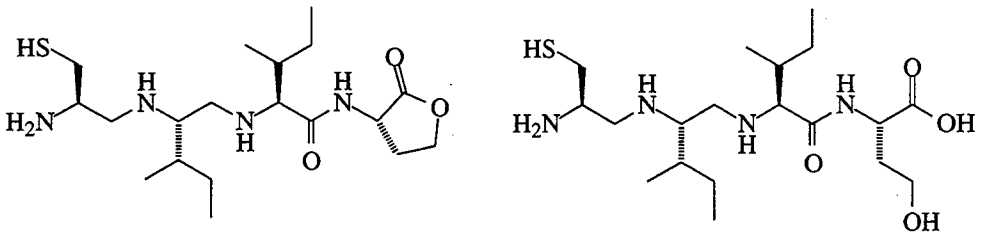

Figure 5.3 Peptide analogs as inhibitors of *ras* farnesyl transferase, **25** and **26**.

More recently, researchers have begun to look in the direction of microbial natural products for farnesyl transferase inhibitors. Several low molecular weight inhibitors have been identified (Figure 5.4).[19]

Use of the inhibitors as probes to elucidate roles of prenylated

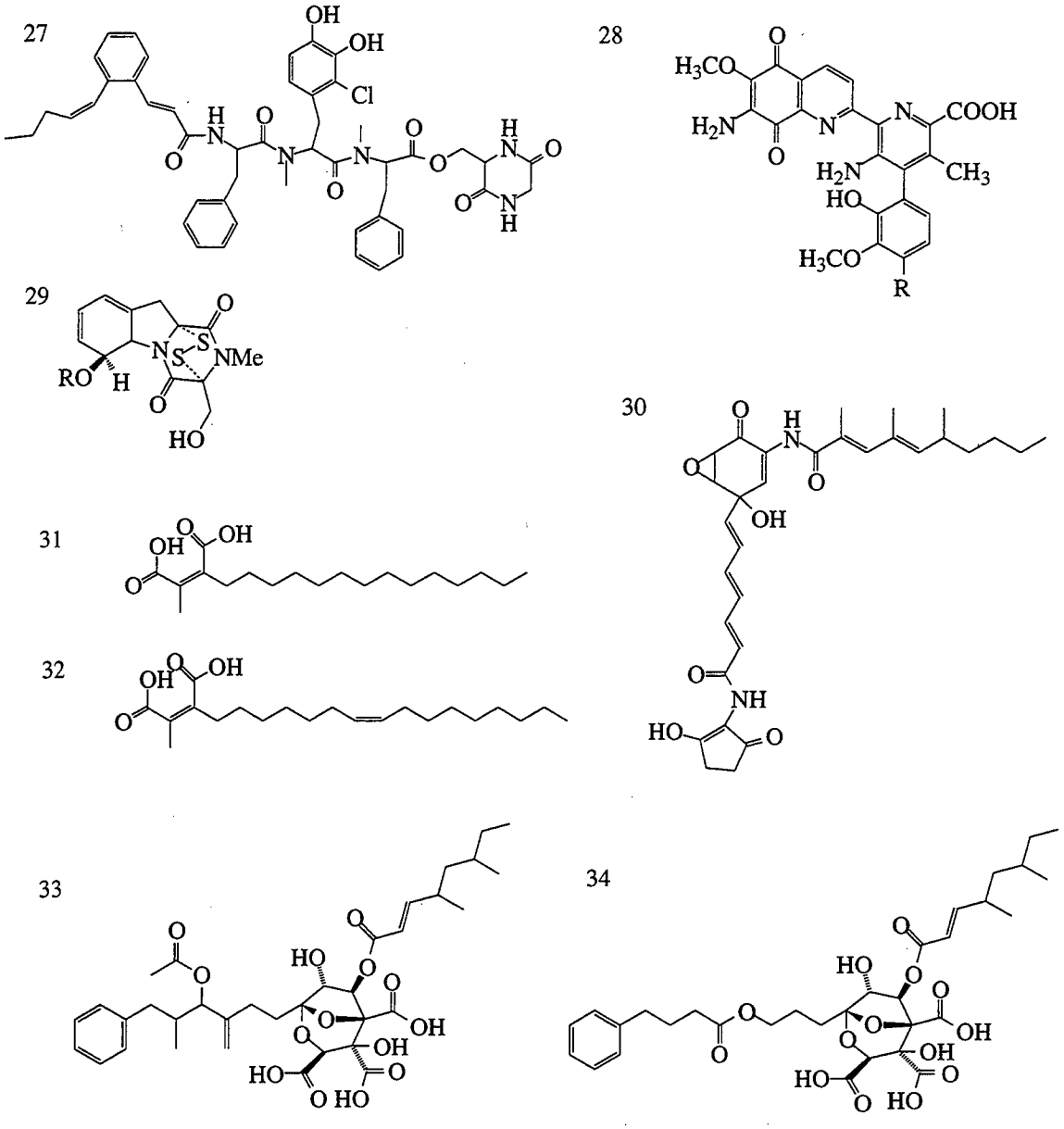

Figure 5.4 Natural products as inhibitors of *ras* farnesyl transferase, **27-34**.[19] (**27**, pepticinnamin E; **28**, streptonigrin; **29**, gliotoxin; **30**, manumycin; **31**, chaetomellic acid A; **32**, chaetomellic acid B; **33**, zaragozic acid A; **34**, zaragozic acid analogue)

proteins has only just begun. Research in this area could not only lead to possible new anticancer drugs, but also help to better understand cell signaling and proliferation. Another critical issue in the search for specific farnesyl transferase inhibitors is the possible effects that an inhibitor may have on the normal functions of other farnesylated proteins, such as nuclear lamins or transducin.[2]

5.3 Results and Discussion

The crude extract of a soil fungus acquired from Boyce Thompson Institute showed greater than 66% inhibition of the *ras* farnesylation transferase enzyme. Of lesser interest was the extract's activity as an antiviral agent against HIV, as an antibiotic against gram positive bacteria and its cytotoxicity. The taxonomy of this soil fungi was characterized by John Bissett of Biosystematics Research Centre of the Central Experimental Farm, Ottawa, Ontario, Canada as *Verticillium tenerum*, the anomorphic form of *Nectria inverta* (now placed in *Verticillium lateritium*).

The fungus was cultured in 250 mL of Sabouraud's Dextrose Broth at 23 °C while shaken at 200 rpm for seven days. Many attempts were made to scale up the fermentations procedure but the activity was lost on each attempt. Thus, 80 L of broth was fermented in small batches (20 flasks per week) over a period of six months. The fermentation was filtered, neutralized and then repeatedly extracted with ethyl acetate. The organic fraction contained the activity as

determined by bioassay. All bioassays were conducted at Schering-Plough Corporation. The sample was initially fractionated on a Sephadex LH-20 column with MeOH as the eluent. The active fraction by bioassay, and later followed with TLC, was further purified by RP-HPLC on a semiprep C18 column using a solvent system of 65:35 MeOH:H_2O. The fraction containing the majority of the activity submitted to further HPLC on a semiprep CN column using an isocratic solvent system of 30% ACN in H_2O . The active fraction was resubmitted to HPLC under the same conditions for the final purification resulting in 8 mg of a pure compound. Unfortunately, the activity decreased after each HPLC step of the purification resulting in an activity of 20 μg/mL. Whether the loss of activity was due to degradation or synergism was not clear.

The structure of the major component of this fraction was finally determined with spectroscopic data. Mass spectra along with the NMR data suggested a molecular formula of $C_{30}H_{28}N_6O_7S_4$. It was apparent that the structure was a dimer, but not a completely symmetric dimer. The ^{13}C NMR spectra indicated the presence of four amide carbonyls, two methine hydroxyls and one methylene hydroxyl which accounted for the seven oxygens. The appearance of a broad band at 3400 cm^{-1} in the IR was also characteristic of hydroxyl groups. The IR spectra showed bands for the amide carbonyls. This evidence along with chemical shifts and an ion in the mass spectra at *m/e* 64 due to the loss of S_2 indicated a epithiodioxopiperazine moiety.

Table 5.1. NMR data for verticillin B

Position	δ^1H	δ^{13}C	HMBC correlations	^{1}H-^{1}H COSY
1, 1'		166.3 (s)		
		166.4 (s)		
3, 3'		73.6 (s)		
		76.6 (s)		
4, 4'		162 (s)		
		163 (s)		
5a, 5a'	5.15 (s, 2H)	83.3 (2d)		
6, 6'	7.5 (s, 2H)			
6a, 6a'		148.8 (2s)		
7, 7'	6.45 (d, 2H)	109.2 (d)		8, 8'
		109.7 (d)		
8, 8'	6.90 (q, 2H)	123.6 (2d)	5a, 5a'	7, 7', 9, 9', 10, 10'
9, 9'	6.60 (t, 2H)	119.3 (2d)		8, 8', 10, 10'
10, 10'	7.30 (d, 2H)	129.5 (d)	6a, 6a', 10a,	8, 8', 9, 9'
		130.1 (d)	10a'	
10a, 10a'		128.1 (s)		
		130.2 (s)		
10b, 10b'		64.9 (2s)		
11, 11'	6.0 (br s, 2H)	81.1 (2d)		
11-OH, 11'-OH	5.80 (s, 2H)			
11a, 11a'		73.7 (s)		
		81.5 (s)		
12, 12'	2.98 (s, 3H),	27.3 (q)	1, 1', 3, 3'	
	3.05 (s, 3H)	27.4 (q)		
13	1.95 (s, 3H)	17.6 (q)	4, 3	
13'	4.25 (dd, 2H)	61.1 (t)	4'	
13'-OH	3.30 (t, 1H)			

Also of interest were the IR spectra, the corresponding UV spectra and the chemical shifts indicating an indole group. With the help of DQ-COSY, HMQC, and HMBC (Table 5.1), the final dimeric structure was proposed (Figure 5.5). Crystallographic studies are being attempted for absolute confirmation of the structure. However, no crystals of crystallographic quality have been obtained yet.

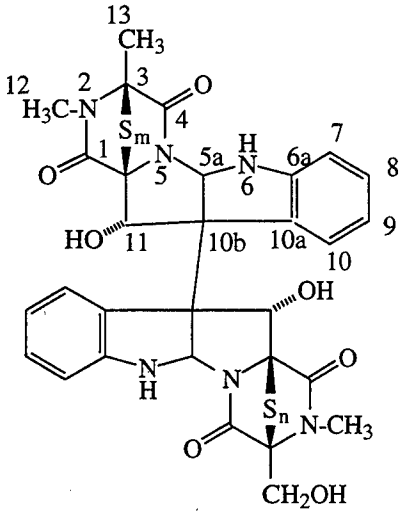

Figure 5.5. Structure of the *ras* farnesylation inhibitor, **35**.

After a literature search, the *ras* farnesylation inhibitor, **35**, isolated from the *V. tenerum* fungal broth was determined to be consistent with the spectroscopic data for verticillin B. *Verticillium* species have been known to produce verticillins A-C (Figure 5.6) which are members of a class of compounds known as the epipolythiodioxopiperazines.[20,21,22] The epipolythiodioxopiperazine toxins (ETP) are produced by a wide range of fungi.[23] These toxins are

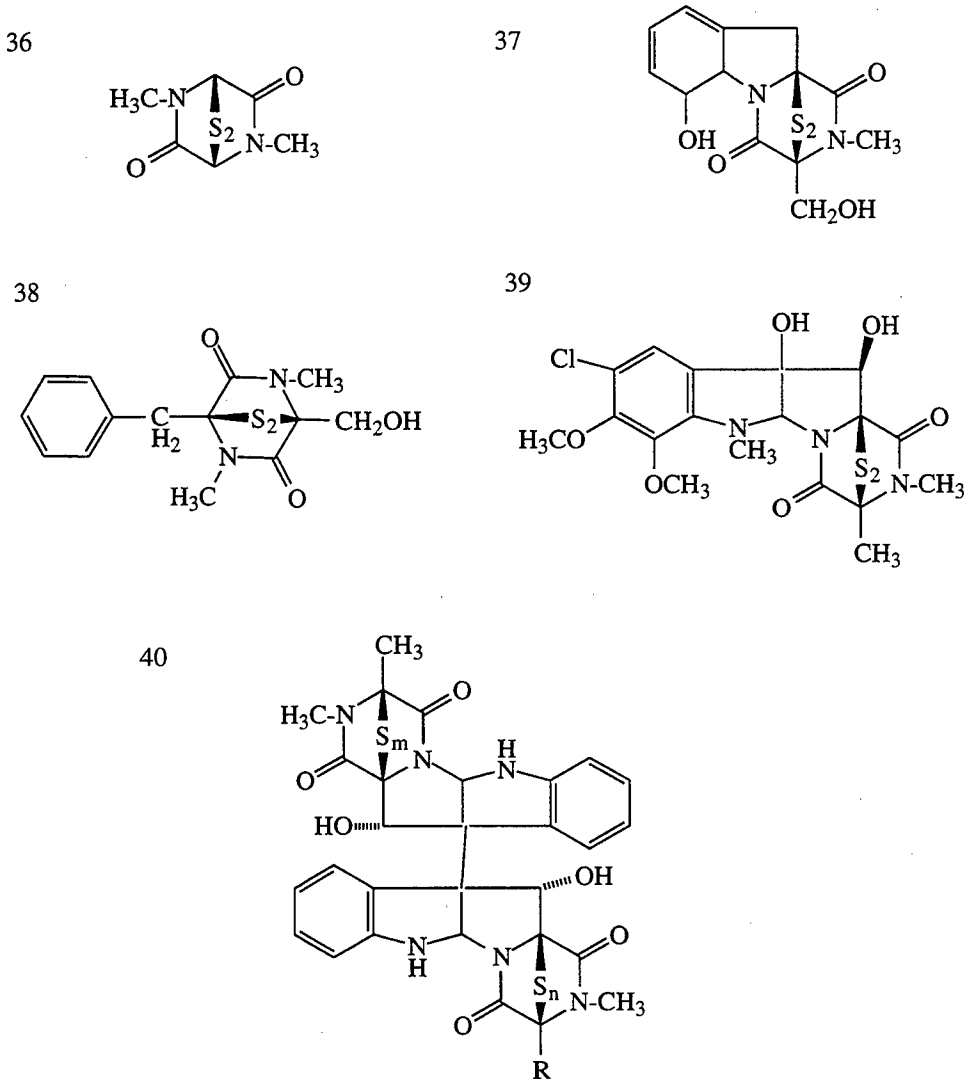

Figure 5.6. Structures of some natural epipolythiodioxopiperazines, **36-40**.[23] (**36**, 1,4-dimethyl-3,6-epidithio-2,5-dioxopiperazine; **37**, gliotoxin; **38**, hyalohendrin; **39**, sporidesmin; **40**, R = CH_3, m = n = 2, verticillin A; R = CH_2OH, m = n = 2, verticillin B; R = CH_2OH, m = 2, n = 3, verticillin C)

characterized as low molecular weight nonpolar molecules with a bridged polysulfide region which confers biological activity.[23] Over 50 naturally occurring ETPs have been isolated and structurally characterized. Some of the structures of epipolythiodioxopiperazines, including the verticillins are shown in Figure 5.6.[24]

ETPs have been well studied due to the range and strength of their biological activities. Their known biological activities include antiviral, antibacterial, antifungal, antiphagocytic, antitumor, and immunosuppressive.[24] In fact, gliotoxin, **37**, is already known to inhibit the *ras* farnesylation enzyme.[19,25] The known activities of the ETPs is in keeping with the original bioassay results of the crude extract. Studies on the molecular variations of both the ETP nucleus and the non-ETP moiety indicate that the ETP nucleus is responsible for most biological activities.[24] The critical role of the sulfur bridged nucleus has been demonstrated by chemical modification which decreases most of the biological activities.[24] ETP polysulfides which contain three or four atoms of sulfur in the sulfur bridge are less abundant but tend to be more toxic than the disulfides even though the higher homologues are probably metabolized to the disulfur compounds within the cells.[24,26] The disulfide bridge is easily reduced to the dithiols and is believed to occur spontaneously at cellular levels of reducing agents. The disulfides and the dithiols are suspected to coexist in cells with mixed disulfides formed between the ETPs and proteinaceous thiols such as *ras* p21.[24] The ETPs are much more active in a range of biological activities than other disulfide compounds

indicating that the piperazinedione ring system provides a more chemically reactive environment for the disulfide bridge.

In vitro studies on the actions of the ETPs on mammalian, fungal and bacterial cells have demonstrated effects on growth processes; in keeping with our observation that verticillin B inhibits the production of the *ras* p21 protein. Previously, it was predicted that the ETP sulfurs would directly modify cellular thiols involved in cell replication.[24] This hypothesis was supported by the fact that many of the ETP react readily with low molecular weight thiols such as dithiothreitol (DTT) and that the presence of these thiol compounds protect the cells against the toxic effects of ETPs.[24] This hypothesis would suggest that the disulfide bridge must be intact for *ras* farnesylation activity. Other studies have shown that reduction of the ETPs to the dithiol form abolishes all biological activity.[24] However, as the ras farnesylation assay is always conducted in the presence of DTT, it is clear why the pure compound shows decreased activity while crude extracts repeatedly were active. The crude mixture probably contained compounds which protected the ETP from reduction.

5.3 Summary

The ras farnesylation inhibitor, verticillin B was isolated from the fungal broth of *V. tenerum*, a soil fungus obtained from Boyce-Thompson Institute. The inhibitor can now be used as a probe to elucidate roles of prenylated proteins. Research in this area could not

only lead to possible new anticancer drugs, but also help to better understand cell signalling and proliferation.

Although inhibitors of *ras* farnesylation transferase are of considerable interest in the study of cell signaling and oncology, ETPs including verticillin B are much too cytotoxic and have too many other biological activities to actually be useful as potential cancer drugs. However, the characterization of a low molecular weight inhibitor is still of use to gain a clearer understanding of the function of the *ras* p21 protein and also may be useful as a lead for developing more specific, less cytotoxic inhibitors.

This work also has significance in that it represents the result of a successful application of a biorational search for a source of biologically active compounds. It is a compelling example of how collaborative, interdisciplinary efforts can lead to exciting developments.

5.4 Experimental

General procedures. NMR spectra were recorded on a Varian XL-400 or a Varian XL-500 spectrometer. Chemical shifts were expressed by δ units in ppm from TMS. IR spectra were recorded on a Mattson IR Spectrophotometer. UV-Vis spectra were obtained from a Shimadzu UV160U UV-Vis Spectrophotometer. MS were obtained from the mass spectrometry facility at Schering-Plough Corporation. CC adsorbent was Sephadex LH-20 (Pharmacia Fine chemicals, Uppsala,

Sweden). TLC was done with glass-backed Si gel plates, 2-25 μ, 250 μ thickness (Aldrich). The HPLC columns employed were a Supelco RPLC-CN semiprep column, 5 μ pore, 10 mm x 25 cm and a Supelco RPLC-C18 semiprep column, 5 μ pore, 10 mm x 25 cm, using a Hewlett-Packard 1050 Series Pump and were monitored with an H-P 1050 Series Multiple Wavelength Dectector at λ = 220 nm. All bioassays were proprietary and were conducted at Schering-Plough Corporation.

Isolation and Structure of Verticillin B. The fungus was cultured in 250 mL of Sabouraud's Dextrose Broth (Difco) in 500 mL erlenmeyer flasks at 23°C while shaken at 200 rpm for seven days. 80 L of broth was fermented in small batches (20 flasks per week) over a period of six months. The fermentation was filtered, neutralized to a pH of 7.0 with NaOH and then repeatedly extracted with EtOAc. The organic fraction was washed with a saturated brine solution, dried over $MgSO_4$ and dried *in vacuo*. The organic fraction contained the activity as determined by bioassay. All bioassays were conducted at Schering Plough. The initially fractionated on a 75 g Sephadex LH-20 column with MeOH as the eluent. The active fraction by bioassay, and later followed with TLC, was further purified by RP-HPLC on a Supelco semiprep C18 column (5μ, 25 cm x 4.6 cm) using a solvent system of 65:35 MeOH:H20 with a flow rate of 2.5 mL/min. The fraction containing the majority of the activity was submitted to further HPLC. The fraction containing the majority of the activity submitted to further HPLC on a Supelco semiprep CN column (5μ, 25 cm x 4.6 cm)

using an isocratic solvent system of 30% ACN in H_2O at a flow rate of 2.5 mL/min. The active fraction was resubmitted to HPLC under the same conditions for the final purification resulting in 8 mg of pure verticillin B. UV(MeOH) λ_{max} 244 nm (ε=69841), 298 (961); IR 3400 br, 2920, 1700, 1698, 1672, 1650, 1354 cm^{-1};^1H NMR (CD_2Cl_2) δ: 1.95 (s, 3H), 2.98 (s, 3H), 3.05 (s, 3H), 3.30 (t, 1H), 4.25 (dd, 2H), 5.15 (s, 2H), 5.80 (s, 2H), 6.0 (br s, 2H), 6.45 (d, 2H), 6.60 (t, 2H), 6.90 (q, 2H), 7.30 (d, 2H), 7.5 (s, 2H); ^{13}C NMR (CD_2Cl_2) δ: 17.6 (q), 27.3 (q), 27.4 (q), 61.1 (t), 64.9 (2s), 73.7 (s),73.6 (s), 76.6 (s), 81.1 (2d), 81.5 (s), 83.3 (2d), 109.2 (d), 109.7 (d), 119.3 (2d), 123.6 (2d), 128.1 (s), 129.5 (d), 130.1 (d), 130.2 (s), 148.8 (2s), 162 (s), 163 (s), 166.3 (s), 166.4 (s); HMQC Correlations (CD_2Cl_2) δ: 2.98-27.3; 3.05-27.4; 1.95-17.6; 4.25-61.6; 5.15-83.3; 6.0-81.1; 6.45-109.2, 109.7; 6.60-119.3; 6.90-123.6, 7.30-129.5, 130.1; HMBC Correlations (CD_2Cl_2) δ: 6.90-83.3; 7.30-148.8, 128.1, 130.2; 2.98-166.3, 73.6; 3.05-166.4, 76.6; 1.95-162, 73.6; 4.25-163; DQ-COSY Correlations (CD_2Cl_2) δ: 6.45-6.90; 6.90-6.60, 7.30; 6.60- 7.30; MS (SIMS) m/z 713 (5), 697 (10), 664 (15), 648 (5), 398 (10), 234 (20), 128 (90), 64 (100%); HRMS (EI^+), ($C_{30}H_{28}N_6O_7S_4$, Δ = ppm).

5.5 References

1. Eisner, *Chemoecology*, **1990**, 1, 38.

2. Hoffman, *Science*, **1991**, 254, 650-651.

3. Alberts,Bray, Lewis, Raff, Roberts, Watson, *Molecular Biology of the Cell*, 2nd ed., Garland Press, **1989**, pp 705.

4. McCormick, In *Oncogenes and the Molecular Origins of Cancer*, Weinberg, Ed., Cold Spring Harbor Laboratory Press, **1989**, pp. 125-145.

5. Hall, *Science*, **1994**, 264, 1413-1414.

6. Stokoe, Macdonald, Cadwallader, Symons, Hancock, *Science*, **1994**, 264, 1463-1467.

7. Grand, Owen, *Biochem. J.*, **1991**, 279, 609-631.

8. Schaber, O'Hara, Garsky, Mosser, Bergstrom, Moores, Marshall, Friedman, Dixon, Gibbs, *J. Biol. Chem.*, **1990**, 256, 14701-14704.

9. Casey, Solski, Der, Buss, *Proc. Natl. Acad. Sci. USA*, **1989**, 86, 8323-8327.

10. Manne, Roberts, Tobin, O'Rourke, De Birgilio, Meyers, Ahmed, Kurz, Resh, Kung, Barbacid, *Proc. Natl. Acad. Sci. USA*, **1990**, 87, 7541-7545.

11. Inglese, Koch, Caron, Lefkowitz, *Nature*, **1992**, 359, 147-150.

12. Volker, Miller, Stock, *Methods: A Companion to Methods in Enzymology*, **1990**, 1, 283-287.

13. Kato, Cox, Hisaka, Graham, Buss, Der, *Proc. Natl. Acad. Sci. USA*, **1992**, 89, 6403-6407.

14. Gibbs, *Cell*, **1991**, 65, 1-4.

15. Travis, *Science*, **1993**, 260, 1877-1888.

16. Reiss, Goldstein, Seabra, Casey, Brown, *Cell*, **1990**, 62, 81-88.

17. Kohl, Mosser, deSolms, Giuliani, Pompliano, Graham, Smith, Scolnick, Oliff, Gibbs, *Science*, **1993**, 260, 1934-1937.

18. James, Goldstein, Brown, Rawson, Somers, McDowell, Crowley, Lucas, Levinson, Marsters, *Science*, **1993**, 260, 1937-1941.

19. Tamanoi, *TIBS*, **1993**, 18, 349-353.

20. Minato, Matsumoto, Katayama, *Chem. Comm.*, **1991**, 44-45.

21. Minato, Matsumoto, Katayama, *J. C. S. Perkin I*, **1973**, 1819-1825.

22. Hauser, Loosli, Niklaus, *Helv. Chim. Acta*, **1972**, 55, 2182-2187.

23. Nagarajan, In *Mycotoxins - Production, Isolation, Separation and Purification*, Betina, Ed, Elsevier Science Publishers, **1984**, pp 351-385.

24. Jordan, Cordiner, *TIPS*, **1987**, 8, 144-149.

25. Van der Pyl, Inokoshi, Shiomi, Yang, Takeshima, Omura, *J. Antibiotics*, **1992**, 45, 1802-1805.

26. Saito, Suzuki, Koyama, Natori, Iitaka, Kinoshita, *Chem. Pharm. Bull.*, **1988**, 36, 1942-1956.

Chapter 6

Isolation and Structure of PDGF Inhibitors from *Cladonia subtenuis*

6.1 Introduction

Chemical prospecting involves the discovery of possible pharmaceutical leads using biorational arguments.[1] The previous chapter showed an example of how collaborative, interdisciplinary efforts can lead to potentially significant developments in unexpected areas. With this idea in mind, a collaborative collecting trip to Archbold Biological Station, Lake Placid, Florida with chemists, mycologists and chemical ecologists from the Cornell Center for Chemical Ecology was arranged. *Cladonia subtenuis* was collected along with some 100 other lichens, fungi and insect samples from Archbold Biological Station. All samples were initially chosen using biological indicators for activity and were immediately submitted to a series of field assays including antimicrobial and cytotoxic assays. Samples were sent to Schering-Plough for further testing with the understanding that Cornell would patent any discoveries, Schering-Plough would have licensing rights to these patents and a percentage

of any money realized from this project would be returned to Archbold Biological Station for conservation.

The extracts of several lichens of the genus *Cladonia* were found to be toxic in the brine shrimp bioassay.[2] When submitted for a further battery of bioassays at Schering-Plough, these crude extracts inhibited the receptor of the platelet-derived growth factor (PDGF), indicating a constituent natural product which could be useful as a drug for the treatment of athersclerosis.

Cardiovascular disease remains the primary cause of death in the US and Western Europe and atherosclerosis, the principal cause of myocardial and cerebral infarction, accounts for the majority of these deaths.[3] Surgical techniques are still the only method in which the majority of atherosclerosis cases are treated. Unfortunately, these approaches have an extraordinarily high failure rate of 30-50%.[4] Recently, there has been remarkable progress in the identification of several different cell types and molecules that are involved in atherogenesis. At the same time, clinical investigations suggest that the lesions of atherosclerosis can be reversed. This result suggests that the ability to antagonize the fibroproliferative response of appropriate molecules such as the growth regulatory molecules could represent a valuable approach toward the treatment and prevention of atherosclerosis.[4] This approach is the direction that the pharmaceutical research group at Schering-Plough Corporation has taken and the extracts of the lichens discussed above were a primary

lead for the discovery of low molecular weight antagonists to the purified receptor for platelet-derived growth factor (PDGF).

Polypeptide growth factors, of which PDGF is just one, play an indispensable role in the proliferation and maintenance of cells.[5] Growth factors are also involved in differentiation, chemotaxis and activation of inflammatory cells and tissue repair. Activation of growth factor receptors leads to gene activation, transcription, and then cell division.[5] An abnormal abundance of growth factors results in diseases characterized by proliferative cellular response or by fibrosis.[4]

PDGF is a glycosylated cationic protein with a molecular weight of 28-32 kD that is dependent upon the extent of glycosylation, which can range from 4-7%. PDGF is a heterodimer made up of A and B chains. PDGF is very basic with a pI of 10.2 and has 16 cysteine residues, all of which are linked by disulfide bonds. All mitogenic activity is lost when PDGF is reduced.[5]

Platelet-derived growth factor is the major mitogenic protein in serum for mesenchymal cells. PDGF is synthesized in megakaryocytes, packaged into platelet α granules, and released from platelets activated by thrombin or at sites of blood vessel injury. Within minutes of platelet binding to the aortic endothelium, PDGF is thought to bind and initiate its biological functions on cells of the blood vessel wall.[5]

The extent of the biological functions of PDGF are many and complicated and not well understood. However, it is clear that the PDGF receptor mediates the signal from the growth factor through its protein tyrosine kinase activity.[6,7] The cell surface receptor for PDGF is an autophosphorylating tyrosine kinase of 180 kD which has a single

hydrophobic membrane-spanning domain, a cytosolic carboxyl terminus and extracellular cysteines.[5] The receptor also contains an extracellular ligand binding domain and an intracellular tyrosine kinase domain responsible for the signaling which functions by phosphorylating protein substrates when activated by PDGF.[7] Phosphorylation of these proteins activates these substrates which then transduce signals to the cell interior. When PDGF binds to its cell surface receptor, serine/threonine kinase activities are activated as well as tyrosine kinases. This network of interacting protein kinases serves as a common mediator leading to DNA synthesis, cell growth and the other varied cellular responses associated with PDGF activation.[5,6,7]

PDGF initiates highly specific but diverse events in target cells bearing the PDGF receptor ranging from significant ion fluxes, increased levels of arachadonic acids and diacylglycerol, stimulated amino acid transport and the morphological rearrangement of actin filaments.[5] Of particular relevance to artherosclerosis is the putative role of PDGF in the inflammatory response.

Much research is being done in the area of inflammation and, although the field is not fully understood, the hypothesis that an injury to the arterial endothelium might precipitate the atherosclerotic process through an excessive inflammatory-fibroproliferative response is currently the accepted hypothesis of atherogenesis.[3,4] For this reason, the role of PDGF in inflammatory and repair processes is of particular interest to the search for a possible treatment of atherosclerosis.

Wound healing involves inflammation and the formation of fibrous lesions in response to injury.[5] The process is, under normal conditions, a protective response to insults to the endothelium and smooth muscle cells, but the development of atherosclerosis through the formation of artherosclerotic fibrous plaques differs from the normal inflammatory response in two respects.[4] First, the principal source of connective tissue in the arterial wall is smooth muscle cells which respond differently to injury than other cell types. There are two different phenotypes of smooth muscle cells, contractile and synthetic. Cells of a contractile phenotype respond to agents that induce either vasoconstriction or vasodilation, such as leukotrienes and NO. Whereas, cells in the synthetic state are capable of producing a number of growth-regulatory molecules and can respond to growth factors by expressing receptors. Observations of smooth muscle cells in atherosclerotic lesions indicate that these cells are mostly in the synthetic phase which can have a profound effect on the response to injury and eventually leading to the fibroproliferative component of this disease process.[4]

Secondly, the sources of arterial injury such as hypercholesterolaemia, hypertension, cigarette smoking, diabetes and obesity are often chronic so the progression the fibroproliferative response is uninterrupted or at least repetitive.[4]

The inflammation process begins with an injury to the arterial walls which results in a dysfunction of the endothelium causing increased trapping of lipoprotein in the artery and the appearance of

specific adhesive glycoproteins on the surface of the endothelial cells.[4] Endothelial injury then promotes platelet adherence and release of platelet constituents including PDGF.[5] PDGF produced by platelets, endothelial cells and smooth muscle cells is a strong chemoattractant for monocytes, neutrophils, fibroblasts, and smooth muscle cells.[3,4,5] Soon monocytes, neutrophils and T-lymphocytes migrate to the area of injury, attach to the glycoproteins and migrate between the endothelial cells. These cells destroy foreign debris and microorganisms, remove injured tissue and mount an immune response by producing more PDGF and other growth factors.[5] At this stage, PDGF is responsible for activation of polymorphonuclear leukocytes and monocytes and the proliferation of smooth muscle cells, macrophages and lymphocytes. Proliferation of connective tissues, such as smooth muscle cells and fibroblasts, leads to the formation of a connective tissue matrix comprised of fibre proteins, collagen, and proteoglycans. As monocytes migrate further beneath the arterial surface, they are converted to macrophages, ingest lipids and eventually become foam cells. PDGF has yet another effect upon the inflammation process; it increases the binding and internalization of lipids forming fatty streaks in the arterial wall.[3,4]

At this point, the arteries contain sites with retracted endothelial cells, which expose underlying lipid-filled macrophages, which, in turn, provide sites for platelet interaction starting the process over again in a chronic cycle.[4]

The progression of advanced fibrous lesions resulting from this excessive inflammatory-fibroproliferative response is marked by the accumulation of alternating layers of smooth muscle cells and lipid-laden macrophages.[3,4] These fibrous plaques may eventually impede the flow of blood or rupture resulting in hemorrhage, thrombosis, and occlusion of the artery. Atherosclerosis can lead to myocardial and cerebral infarction, gangrene and loss of function in the extremities. Occlusive lesions of atherosclerosis can sometimes be clinically reversed after *aggressive* treatment with lipid-lowering drugs and diet control. On the other hand, the principal surgical approaches to the treatment are bypass grafting and angioplasty have a failure rate of 30-50% because surgery tends to be yet another form of arterial injury.[3,4]

Due to the lack of effective treatment for atherosclerosis, pharmaceutical companies have begun to look for more effective therapeutic agents. Antagonists to one of the several of the growth regulatory molecules such as PDGF represent a possible approach towards treatment and prevention of this disease. Because antibodies to the PDGF receptor are known to help decrease the production of atherosclerotic plaques, Schering-Plough Corporation has chosen to focus on the search for an inhibitor of the PDGF receptor.[4]

As of yet, the only known inhibitors of the PDGF receptor are large peptides. Peptides are poor leads for drugs for several reasons including low bioavailability and poor solubility. Thus, a low molecular weight nonpeptidal inhibitor would be of considerable

importance as a lead for a drug and as a probe for understanding the aetiology and pathogenesis of atherosclerosis.

6.2 Results and Discussion

Cladonia subtenuis was collected in Lake Placid, Florida at the Archbold Biological Station. The lichens were air-dried. Later, the crude extracts were prepared through a process of extracting, pulverizing and filtering successively in increasingly polar solvents. The active component was purified using bioassay-guided fractionation. All bioassays were performed at Schering-Plough Corporation and were tests of inhibition of the PDGF receptor. The crude extract was initially partitioned with a modified Kupchan scheme. As the hexane and dichloromethane fractions contained most of the activity, these fractions were combined and submitted to fractionation on a Sephadex LH-20 column. Two fractions were found to contain activity.

The first fraction was crystallized from a 1:1 mixture of methanol and dichloromethane. The spectroscopic data suggested a depside, two aromatic rings connected by an ester. The proton NMR contained 10 singlets; three aromatic methyls, one methyl ester, two aromatic protons, three hydroxyl groups and an aldehyde. Thus, the structure appeared to be a depside with these substituents. In order to determine substitution pattern on the aromatic rings, a crystallographic study was done. The x-ray structure revealed this compound to be a

para-depside, atranorin (Figure 6.1). Depsides, including atranorin, are well studied metabolites of lichens.[8] However, as this compound turned out to be only marginally active, the purification process was continued to determine the structure of the more active component(s).

After many difficulties, a second active metabolite was finally purified through reverse-phase HPLC. The purification process was difficult to monitor due to a lack of UV absorbance. This compound was of more interest due to its high activity (5 μg/mL) as well as being the first small molecule found to inhibit this receptor in the Schering assay.

The proton and carbon NMR were interesting in having one signal in each spectra. The ^{1}H NMR spectra had a singlet at δ 3.48 ppm which correlated to the only carbon at δ 60 ppm in the ^{13}C spectra. As the compound was not appreciably volatile, these data indicated a high degree of symmetry in the molecule and the presence of a number of heteroatoms. The ratio m/m+1 in the mass spectra indicated 10-11 carbons in the molecule. As there was no indication of an A+2 ion, the possibility of a cyclic polysulfide was eliminated. The only molecular formula which was consistent with a molecular ion of 220 and also fulfilled the heteroatom and symmetry requirements was $C_{15}H_{20}O_5$. With this molecular formulaas a target, the structure was proposed to be the crown ether, 15-crown-5 (Figure 6.2). All the spectral data agreed with the published data for crown ethers.[9,10,11,12] High resolution mass spectrometry

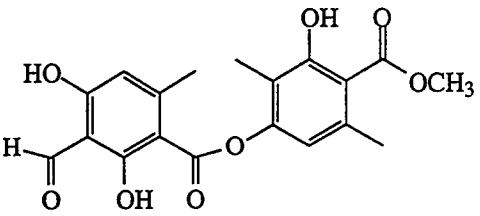

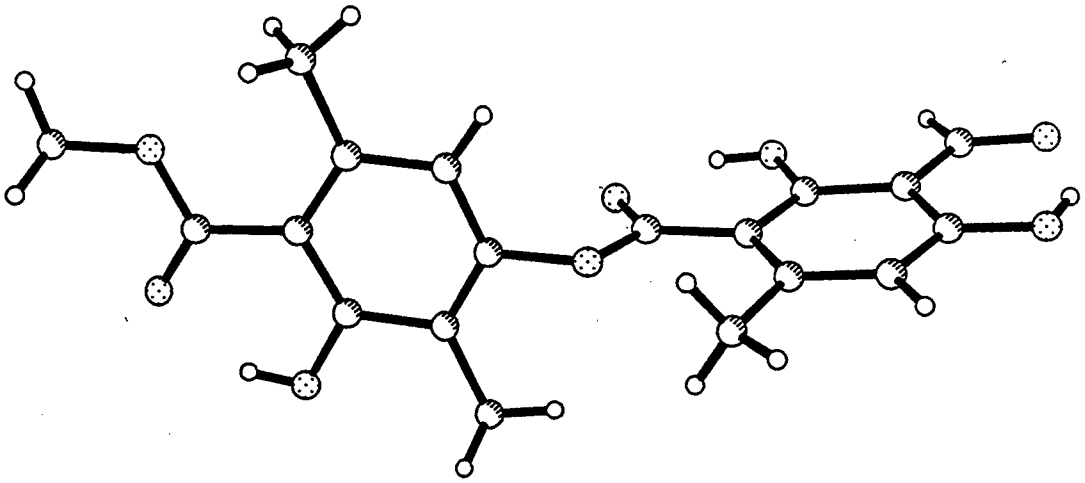

Figure 6.1 Computer generated model of atranorin, **41**.

or X-ray crystallography would definitively confirm the structure, and such experiments are planned in the future.

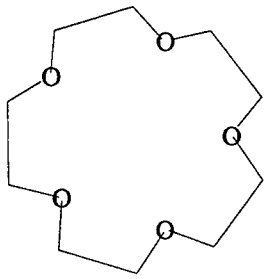

Figure 6.2 Proposed structure of the inhibitor of the PDGF receptor, **42**.

Assuming the formulation as 15-crown-5 to be correct, clearly authentic material should be submitted to the bioassay. This has been done, but results are not yet available. Should this data continue to support 15-crown-5, an important future goal will be figuring out its origin, which could be artifactual.

6.3 Summary

The secondary metabolites of lichens have been of interest for quite some time due to their activity in many bioassays. The varied and unique structures derived from lichens are proposed to fulfill three biological functions; antimicrobial, allelopathic and antiherbivore. The putative roles of these natural products are supported by the available evidence. Lichens grow very slowly, yet manage to compete efficiently. The competitiveness of lichens could

be due to the fact that they produce a variety of compounds which are antimicrobial, allelopathic to vascular plants or that inhibit the growth of lichens, mosses and liverworts. Lichens also deter feeding of generalist herbivores despite their availability as food suggesting the presence of secondary metabolites which are capable of defending lichens from herbivory.[13]

Interestingly, atranorin and other depsides have long been known to inhibit the growth of bryophytes and other lichens.[13] Atranorin is also known to significantly decrease the herbivory and growth of insect pests. In light of this information, it is not surprising to find that atranorin was found to be toxic to brine shrimp and have marginal inhibitory activity against the PDGF receptor.

Crown ethers are well known compounds first synthesized by Pederson at Dupont.[14] However, a literature search indicated that this work would be the first report of such a compound from a natural source. However, the possibility remains that this compound could also be an artifact of the isolation procedure. The isolation of known synthetic compounds from a natural source has been previously reported in such cases as cyclodextrins and paracyclophanes.[15,16]

Crown ethers are good chelators of cations.[14] In particular, the cavity created by 15-crown-5 accomodates Na^+ extremely well and is known to interrupt some cell processes. Structures of the antibiotics such as tricothecene, halicondrin, valinomycin, and nonactin, which also chelate cations, have often been compared to crown ethers.[17,18]

Two other lichens of the genus *Cladonia* also exhibited inhibitory activity against the PDGF receptor. In the search for other low molecular weight inhibitors, these lichens should be examined for the production of new inhibitors or possible analogs of 42.

Atranorin and 15-crown-5 were both isolated from the lichen, *Cladonia subtenuis* collected at Archbold Biological Station, Lake Placid, Florida. The inhibitors can now be used as probes to elucidate the role of PDGF in atherosclerosis. Research in this area could not only lead to possible new cardiovascular treatments, but also help to better understand atherogenesis. Although inhibitors of the PDGF receptor are of considerable interest in the study of atherogenesis, these compounds are not active enough to actually be useful as potential drugs for atherosclerosis.

This work also has significance in that it represents the result of a successful application of a biorational search for a source of biologically active compounds. It is a compelling example of how collaborative, interdisciplinary efforts can lead to exciting developments.

6.4 Experimental

General procedures. NMR spectra were recorded on a Varian XL-400 or a Varian XL-500 spectrometer. Chemical shifts were expressed by δ units in ppm from TMS. IR spectra were recorded on a Mattson IR Spectrophotometer. UV-Vis spectra were obtained from a

Shimadzu UV160U UV-Vis Spectrophotometer. MS were obtained from the mass spectrometry facility at Schering-Plough Corporation. CC adsorbent was Sephadex LH-20 (Pharmacia Fine chemicals, Uppsala, Sweden). The HPLC columns employed were a Supelco RPLC-CN analytical column, 5 μ pore, 2.3 mm x 25 cm using a Hewlett-Packard 1050 Series Pump and were monitored with an H-P 1050 Series Multiple Wavelength Detector at λ = 215 nm. All PDGF receptor bioassays are proprietary and were conducted at Schering-Plough Corporation.

Brine Shrimp Bioassay. Sea water was prepared at 38 g sea salt per liter of water. Sea water was put in a small divided tank and shrimp eggs were added to one side and covered. The light of the lamp on the other side attracts the shrimp to swim through the perforations after they hatch. After two days, when the shrimp larvae are ready, 5 mL of seawater was added each test vial and 10 shrimp were added per vial. Each extract was tested at 10 mg/mL in 50 μL of DMSO. 24 hours later, the number of survivors were recorded. 50 μL of DMSO was used as a control sample.[2]

Purification and Structure of Atranorin. *Cladonia subtenuis* was collected at Archbold Biological Station, Lake Placid, Florida. The lichens were air-dried. Later, the crude extracts were prepared through a process of extracting, pulverizing and filtering successively in increasingly more polar solvents. The crude extract was initially

partitioned with a modified Kupchan scheme. First, the crude was partitioned between Hex and 90% MeOH:$H_2$0. The MeOH:H20 phase was diluted to 70% MeOH:H_2O and extracted with CH_2Cl_2. The MeOH:$H_2$0 phase was again diluted to 50% MeOH:$H_2$0 and extracted with EtOAc. As the hexane and dichloromethane fractions contained most of the activity, these fractions were combined and submitted to fractionation on a Sephadex LH-20 column. Two fractions were found to contain activity. Atranorin was crystallized from a 1:1 mixture of methanol and dichloromethane. ^{1}H NMR (THF-d8) δ: 1.70 s (3H), 2.02 s (3H), 2.68 s (3H), 3.98 s (3H), 6.42 s (1H), 6.63 s (1H), 10.35 s (1H), 10.88 s (2H), 11.92 s (1H); ^{13}C NMR (THF-d8) δ: 9.3, 23.8, 24.9, 52.5, 105.0, 109.3, 110.9, 112.6, 112.8, 117.0, 117.1, 117.4, 117.5, 140.3, 152.9, 153.3, 163.5, 173.0, 194.3.

Single crystal X-ray structure determination of atranorin. Atranorin was crystallized as colorless needles from a 1:1 mixture of methanol and dichloromethane, and a single crystal with dimensions 0.10 x 0.10 x. 0.50 mm was selected for analysis. All measurements were done on a Siemens R3m diffractometer using graphite monochromated CuKα radiation (λ = 1.54180 Å). Preliminary diffraction photographs displayed orthorhombic symmetry, and accurate lattice constants of a = 12.117(9), b = 15.33(3), c = 18.83(2) Å were determined by a least-squares fit of 25 diffractometer-measured 2θ values in the range of 35-45°. Systematic extinctions, crystal density, and optical activity were uniquely consistent with space group P_{bca}

with one molecule of composition $C_{19}H_{18}O_8$ forming the asymmetric unit. A total of 2042 reflections with $2\theta \leq 100°$ were collected using a variable speed θ:2θ scan. No absorption or decomposition corrections were made. After correction for Lorentz, polarization, and background effects, 1300 of the 2042 unique reflections were judged observed ($|F_0| \geq 4\sigma |F_0|$). The structure was solved by direct methods and refined by full-matrix least-squares using the SHELXTL program set. Anisotropic thermal parameter were employed for the nonhydrogen atoms and the hydrogen atoms rode on the heavy atoms with fixed geometry. The final agreement was R = 0.055.

Purification and Structure of 42. *Cladonia subtenuis* was collected in Florida at the Archbold State Preserve. The lichens were air-dried. Later, the crude extracts were prepared through a process of extracting, pulverizing and filtering successively in increasingly more polar solvents. The crude extract was initially partitioned with a modified Kupchan procedure. First, the crude was partitioned between hexane and 90% MeOH:H_20. The MeOH:H20 phase was diluted to 70% MeOH:H_2O and extracted with CH_2Cl_2. The MeOH:H_20 phase was again diluted to 50% MeOH:H_20 and extracted with EtOAc. As the hexane and dichloromethane fractions contained most of the activity, these fractions were combined and submitted to fractionation on a Sephadex LH-20 column. Two fractions were found to contain activity. After many difficulties, a second active metabolite was finally purified through reverse-phase HPLC. The active fraction from column

chromatography was initally fractionated on a Supelco analytical RP-LCCN column (5 μ pore, 25 cm x 2.3 mm) with 35:65:0.1 ACN:H_2O:HOAc as the eluent with a flow rate of 1.5 mL/min. After 25 min, the column was flushed with 45:55:0.1 ACN:H_2O:HOAc. Due to the lack of UV absorbence, chromatography was monitored at λ = 210 nm with very high sensitivity. The two fractions that were active from this fractionation were further submitted to purification on the same column using 35:65:0.1 MeOH:H_2O:HOAc as the eluent with a flow rate of 1.0 mL/min yielding 3 mg of pure compound. The final compound was active at a concentration of 5 μg/mL. ^1H NMR ($CDCl_3$) δ: 3.55 s; ^{13}C NMR (CD_2Cl_2)δ: 60; HMQC Correlations: δ 3.55-77 ppm; IR ν: cm^{-1}. MS (SIMS) m/z 221 (80).

6.5 References

1. Eisner, *Chemoecology*, **1990**, 1, 38.

2. Meyer, Ferrigini, Putnam, Jacobson, Nichols, McLaughlin, *Planta Medica* **1982**, 45, 31-32.

3. Ross, *N. Engl. J. Med.*, **1986**, 314, 488-500.

4. Ross, *Nature*, **1993**, 362, 801-809.

5. Deuel, *Ann. Rev. Cell Biol.*, **1987**, 3, 443-492.

6. Aaronson, *Science*, **1991**, 254, 1146-1153.

7. Cantley, Auger, Carpenter, Duckworth, Graziani, Kapeller, Soltoff, *Cell*, **1991**, 64, 281-302.

8. Brassy, Bachet, Bodo, Molho, *Acta Cryst.*, **1982**, B38, 3126-3128.

9. Belton, Tanner, Wright, Payne, Truter, Wingfield, *J. Chem. Soc., Perkin 2*, **1985**, 1307-1311.

10. Buchanan, Mathias, Bensimon, Charland, *Can. J. Chem.*, **1992**, 70, 981-991.

11. Aldrich Library of NMR Spectra, Pouchert, Ed., **1983**, Aldrich Chemical Company, pp 212.

12. Aldrich Library of IR Spectra, Pouchert, Ed., **1981**, Aldrich Chemical Company, pp 147.

13. Lawrey, *The Bryologist*, **1986**, 89, 111-122.

14. Pederson, *Science*, **1988**, 241, 536-540.

15. Moore, Chen, Patterson, Moore, Brinen, Kato, Clardy, *J. Am. Chem. Soc.*, **1990**, 112, 4061-4063.

16. Entzeroth, Moore, Niemczura, Patterson, Shoolery, *J. Org. Chem.*, **1986**, 51, 5307-5310.

17. Hirata, Uemara, *Pure and Appl. Chem.*, **1986**, 58, 701-710.

18. Anderson, Ashton, Black, Leigh, Slawin, Stoddart, Williams, *J. Chem. Soc., Chem. Comm.*, **1989**, 13, 904-908.

Appendix A

Tables of X-ray Crystallographic Results for

Syringolide 2

Table A.1 Structure determination summary for syringolide 2.

Crystal Data

Empirical Formula	$C_{15}\ H_{24}\ O_6$
Color; Habit	colorless plates
Crystal Size (mm)	0.05 x 0.2 x 0.54
Crystal System	Monoclinic
Space Group	$P2_1$
Unit Cell Dimensions	$\underline{a}$ = 8.0720(10) Å
	$\underline{b}$ = 5.7850(10) Å
	$\underline{c}$ = 16.773(4) Å
	β = 90.39(2)°
Volume	783.2(2) $Å^3$
Z	2
Formula weight	300.3
Density(calc.)	1.274 Mg/m^3
Absorption Coefficient	0.775 mm^{-1}
F(000)	324

Table A.2 Data collection for syringolide 2.

Diffractometer Used	Siemens R3m/V
Radiation	CuKα (λ = 1.54178 Å)
Temperature (K)	296
Monochromator	Highly oriented graphite crystal
2θ Range	4.0 to 116.0^{o}
Scan Type	2θ–θ
Scan Speed	Variable; 1.50 to 29.30^{o}/min. in ω
Scan Range (ω)	0.50^{o} plus Kα–separation
Background Measurement	Stationary crystal and stationary counter at beginning and end of scan, each for 37.5% of total scan time
Standard Reflections	3 measured every 50 reflections
Index Ranges	$-8 \leq h \leq 8$, $0 \leq k \leq 6$ $0 \leq \ell \leq 18$
Reflections Collected	1247
Independent Reflections	1200 (R_{int} = 2.38%)
Observed Reflections	1173 ($F > 4.0\sigma(F)$)
Absorption Correction	N/A

Table A.3 Solution and refinement for syringolide 2.

System Used	Siemens SHELXTL PLUS (VMS)
Solution	Direct Methods
Refinement Method	Full-Matrix Least-Squares
Quantity Minimized	$\sum w(F_o - F_c)^2$
Absolute Structure	N/A
Extinction Correction	N/A
Hydrogen Atoms	Riding model, fixed isotropic U
Weighting Scheme	Unit weights
Number of Parameters refined	190
Final R indices (obs. data)	R = 5.01 %, wR = 7.21 %
R Indices (all data)	R = 5.11 %, wR = 7.24 %
Goodness-of-Fit	0.98
Largest and Mean Δ/σ	0.139, 0.015
Data-to-Parameter Ratio	6.2:1
Largest Difference Peak	0.18 $eÅ^{-3}$
Largest Difference Hole	-0.26 $eÅ^{-3}$

Table A.4 Atomic coordinates ($x10^4$) and equivalent isotropic displacement coefficients ($Å^2x10^3$) for syringolide 2. The standard deviation of the least significant figure of each distance is given in parentheses.

	x	y	z	U(eq)
O(2)	9002(5)	2015(910)	3361(3)	35(2)
O(6)	9900(6)	6806(910)	4210(3)	45(2)
O(3)	11763(6)	938(910)	3191(3)	35(2)
O(1)	8543(6)	7253(910)	3062(4)	55(2)
O(4)	14896(7)	1949(910)	4724(3)	57(2)
O(5)	13875(6)	5478(910)	3656(3)	36(2)
C(5)	8904(10)	3225(910)	1594(5)	50(3)
C(1)	9680(9)	6399(910)	3425(5)	38(3)
C(3)	10445(8)	2380(910)	2901(4)	33(2)
C(4)	10240(9)	1819(910)	2030(4)	43(3)
C(5')	14889(9)	3532(910)	3407(5)	44(3)
C(3')	12430(8)	1928(910)	3909(4)	31(2)
C(8)	7065(10)	2828(910)	-560(4)	56(3)
C(2')	12243(9)	4555(910)	3813(4)	28(2)
C(2)	11032(8)	4860(910)	3101(4)	30(2)
C(7)	7397(11)	3757(910)	279(5)	57(3)
C(6)	8724(10)	2447(910)	731(5)	55(3)
C(4')	14322(9)	1564(910)	3926(5)	39(3)
C(1')	11474(9)	5897(910)	4502(4)	37(3)
C(9)	5635(11)	4041(910)	-981(5)	64(4)
C(10)	5243(12)	3081(909)	-1789(5)	80(5)

* Equivalent isotropic U defined as one third of the trace of the orthogonalized U_{ij} tensor

Table A.5 Bond lengths (Å) for syringolide 2.

O(2)-C(3)	1.417 (168)
O(6)-C(1')	1.457 (280)
O(3)-C(3')	1.435 (304)
O(4)-C(4')	1.429 (170)
O(5)-C(2')	1.446 (285)
C(5)-C(6)	1.523 (239)
C(3)-C(4)	1.506 (195)
C(5')-C(4')	1.507 (551)
C(3')-C(4')	1.542 (155)
C(8)-C(9)	1.521 (343)
C(2')-C(1')	1.528 (375)
C(9)-C(10)	1.496 (285)
O(6)-C(1)	1.349 (183)
O(3)-C(3)	1.434 (424)
O(1)-C(1)	1.204 (313)
O(5)-C(5')	1.455 (563)
C(5)-C(4)	1.532 (390)
C(1)-C(2)	1.513 (430)
C(3)-C(2)	1.547 (685)
C(3')-C(2')	1.535 (736)
C(8)-C(7)	1.528 (273)
C(2')-C(2)	1.549 (146)
C(7)-C(6)	1.511 (370)

Table A.6 Bond angles (°) for syringolide 2.

C(1)-O(6)-C(1')	112.0(134)
C(5')-O(5)-C(2')	106.3(418)
O(6)-C(1)-O(1)	121.1(304)
O(1)-C(1)-C(2)	127.6(156)
O(2)-C(3)-C(4)	114.3(91)
O(2)-C(3)-C(2)	105.8(285)
C(4)-C(3)-C(2)	116.2(289)
O(5)-C(5')-C(4')	104.2(202)
O(3)-C(3')-C(4')	109.1(121)
C(7)-C(8)-C(9)	113.2(294)
O(5)-C(2')-C(2)	112.9(205)
O(5)-C(2')-C(1')	108.9(300)
C(2)-C(2')-C(1')	105.5(214)
C(1)-C(2)-C(2')	104.1(185)
C(8)-C(7)-C(6)	113.9(265)
O(4)-C(4')-C(5')	109.0(320)
C(5')-C(4')-C(3')	101.0(266)
C(8)-C(9)-C(10)	113.9(254)
C(3)-O(3)-C(3')	109.0(342)
C(4)-C(5)-C(6)	111.0(237)
O(6)-C(1)-C(2)	111.3(141)
O(2)-C(3)-O(3)	109.8(205)
O(3)-C(3)-C(4)	106.3(209)
O(3)-C(3)-C(2)	103.9(231)
C(5)-C(4)-C(3)	114.9(284)
O(3)-C(3')-C(2')	105.7(258)
C(2')-C(3')-C(4')	103.5(276)
O(5)-C(2')-C(3')	107.2(253)
C(3')-C(2')-C(2)	104.8(296)
C(3')-C(2')-C(1')	117.6(230)
C(1)-C(2)-C(3)	113.8(191)
C(3)-C(2)-C(2')	104.6(346)
C(5)-C(6)-C(7)	113.0(290)
O(4)-C(4')-C(3')	108.1(149)
O(6)-C(1')-C(2')	106.7(116)

Table A.7 Anisotropic displacement coefficients ($Å^2x10^3$) for syringolide 2. The standard deviation of the least significant figure of each distance is given in parentheses.

	U_{11}	U_{22}	U_{33}	U_{12}	U_{13}	U_{23}
O(2)	27(3)	23(3)	56(3)	-2(3)	1(2)	-1(3)
O(6)	37(3)	40(3)	58(3)	8(3)	2(2)	-13(3)
O(3)	31(3)	27(3)	47(3)	8(2)	-11(2)	-8(3)
O(1)	35(3)	27(3)	101(5)	6(3)	-30(3)	-7(4)
O(4)	61(3)	54(4)	57(4)	-2(4)	-32(3)	5(4)
O(5)	25(3)	34(3)	48(3)	-5(3)	-7(2)	2(3)
C(5)	48(5)	55(6)	48(5)	8(5)	-13(4)	-8(5)
C(1)	31(4)	16(5)	68(6)	-2(4)	-4(4)	-5(4)
C(3)	28(4)	26(5)	45(4)	5(4)	-6(3)	-3(4)
C(4)	42(4)	44(5)	43(4)	6(5)	-10(3)	-7(5)
C(5')	25(4)	49(6)	58(5)	3(4)	-4(4)	0(5)
C(3')	30(4)	22(4)	39(4)	3(4)	-6(3)	0(4)
C(8)	58(5)	73(8)	36(4)	-1(6)	1(4)	-1(5)
C(2')	26(4)	27(4)	31(4)	-2(4)	-4(3)	2(4)
C(2)	26(4)	32(5)	33(4)	0(4)	-8(3)	1(4)
C(7)	54(5)	70(7)	46(5)	2(6)	-6(4)	-4(5)
C(6)	51(5)	70(8)	43(4)	6(6)	-10(4)	-8(5)
C(4')	33(4)	33(5)	51(5)	6(4)	-12(3)	1(4)
C(1')	44(4)	29(5)	38(4)	4(4)	-3(3)	0(4)
C(9)	55(6)	86(9)	51(5)	4(6)	-4(4)	-3(6)
C(10)	77(7)	117(11)	45(5)	-2(8)	-13(5)	-2(7)

The anisotropic displacement exponent takes the form:

$-2\pi^2(h^2a^{*2}U_{11} + \ldots + 2hka^*b^*U_{12})$

Table A.8 Proton-atom coordinates ($x10^4$) and isotropic displacement coefficients ($Å^2x10^3$) for syringolide 2. The standard deviation of the least significant figure of each distance is given in parentheses.

	x	y	z	U
H(2A)	8710	607	3326	80
H(4A)	14909	3392	4819	80
H(5A)	9192	4835	1609	80
H(5B)	7864	3039	1862	80
H(4B)	11280	2071	1769	80
H(4C)	9976	208	1979	80
H(5'A)	16044	3850	3492	80
H(5'B)	14708	3186	2854	80
H(3'A)	11899	1354	4380	80
H(8A)	6821	1207	-525	80
H(8B)	8049	3001	-872	80
H(2B)	11571	5562	2653	80
H(7A)	6387	3699	578	80
H(7B)	7723	5349	240	80
H(6A)	8462	828	721	80
H(6B)	9764	2651	466	80
H(4'A)	14644	80	3723	80
H(1'A)	11299	4895	4950	80
H(1'B)	12191	7136	4665	80
H(9A)	5903	5650	-1035	80
H(9B)	4665	3931	-655	80
H(10A)	4335	3923	-2020	80
H(10B)	6197	3219	-2124	80
H(10C)	4945	1481	-1740	80

Appendix B

Tables of X-ray Crystallographic Results for

Atranorin

Table B.1 Structure determination summary for atranorin.

Crystal Data

Empirical Formula	$C_{19}H_{18}O_8$
Color; Habit	Colorless, needle
Crystal Size (mm)	0.10 x 0.10 x 0.50
Crystal System	Orthorhombic
Space Group	Pbca
Unit Cell Dimensions	$\underline{a}$ = 12.117(9) Å
	$\underline{b}$ = 15.33(3) Å
	$\underline{c}$ = 18.83(2) Å
Volume	3497(9) $Å^3$
Z	8
Formula weight	374.3
Density(calc.)	1.422 Mg/m^3
Absorption Coefficient	0.905 mm^{-1}
F(000)	1568

Table B.2 Data collection for atranorin.

Diffractometer Used	Siemens R3m/V
Radiation	CuKα (λ = 1.54178 Å)
Temperature (K)	296
Monochromator	Highly oriented graphite crystal
2θ Range	3.0 to 100.0°
Scan Type	2θ–θ
Scan Speed	Variable; 2.19 to 29.30°/min. in ω
Scan Range (ω)	0.50° plus Kα-separation
Background Measurement	Stationary crystal and stationary counter at beginning and end of scan, each for 25.0% of total scan time
Standard Reflections	3 measured every 50 reflections
Index Ranges	$-12 \leq h \leq 0$, $-15 \leq k \leq 0$ $0 \leq \ell \leq 18$
Reflections Collected	2042
Independent Reflections	1757 (R_{int} = 0.00%)
Observed Reflections	1300 ($F > 4.0\sigma(F)$)
Absorption Correction	N/A

Table B.3 Solution and refinement for atranorin.

System Used	Siemens SHELXTL PLUS (VMS)
Solution	Direct Methods
Refinement Method	Full-Matrix Least-Squares
Quantity Minimized	$\sum w(F_o - F_c)^2$
Absolute Structure	N/A
Extinction Correction	N/A
Hydrogen Atoms	Riding model, fixed isotropic U
Weighting Scheme	$w^{-1} = \sigma^2(F) + 0.0010F^2$
Number of Parameters refined	244
Final R indices (obs. data)	R = 5.48 %, wR = 8.00 %
R Indices (all data)	R = 7.70 %, wR = 8.73 %
Goodness-of-Fit	1.94
Largest and Mean Δ/σ	0.001, 0.000
Data-to-Parameter Ratio	5.3:1
Largest Difference Peak	0.21 $eÅ^{-3}$
Largest Difference Hole	-0.22 $eÅ^{-3}$

Table B.4 Atomic coordinates ($x10^4$) and equivalent isotropic displacement coefficients ($Å^2x10^3$) for atranorin. The standard deviation of the least significant figure of each distance is given in parentheses.

	x	y	z	U(eq)
O(1)	1863(3)	7572(2)	1023(2)	62(1)
C(2)	1213(3)	9011(3)	855(2)	42(2)
O(3)	874(2)	4636(2)	1312(2)	67(1)
O(4)	-127(3)	9593(2)	1660(2)	71(1)
O(5)	514(3)	8033(2)	1729(2)	69(1)
C(6)	607(4)	10532(3)	804(3)	54(2)
C(7)	2205(3)	5259(3)	2137(2)	45(2)
C(8)	1901(4)	9158(3)	265(3)	49(2)
O(9)	1746(3)	3774(2)	2296(2)	70(2)
C(10)	562(4)	9685(3)	1111(3)	50(2)
C(11)	1142(4)	8177(3)	1240(3)	47(2)
O(12)	2997(3)	4359(2)	3008(2)	74(2)
C(13)	1475(4)	5319(3)	1553(3)	48(2)
C(14)	1912(4)	6783(3)	1408(3)	50(2)
C(15)	1326(4)	6094(3)	1169(3)	51(2)
C(16)	2646(4)	6758(3)	1966(3)	56(2)
O(17)	1396(3)	11417(2)	-91(2)	83(2)
C(18)	1926(4)	9965(4)	-39(3)	61(2)
C(19)	2818(4)	5991(3)	2337(3)	50(2)
C(20)	1303(4)	10641(3)	226(3)	57(2)
C(21)	2286(4)	4400(3)	2478(3)	52(2)
C(22)	3667(5)	6008(3)	2911(3)	82(2)
O(23)	-29(3)	11974(3)	826(2)	96(2)
C(24)	2622(4)	8483(3)	-69(3)	72(2)
C(25)	574(4)	6126(3)	541(3)	75(2)
C(26)	-44(5)	11222(4)	1083(3)	80(3)
C(27)	3139(6)	3530(3)	3351(3)	95(3)

* Equivalent isotropic U defined as one third of the trace of the orthogonalized U_{ij} tensor

Table B.5 Bond lengths (Å) for atranorin.

O(1)-C(11)	1.338 (6)
C(2)-C(8)	1.406 (7)
C(2)-C(11)	1.472 (7)
O(4)-C(10)	1.336 (6)
C(6)-C(10)	1.422 (8)
C(6)-C(26)	1.421 (9)
C(7)-C(19)	1.397 (7)
C(8)-C(18)	1.364 (8)
O(9)-C(21)	1.211 (7)
O(12)-C(27)	1.436 (7)
C(14)-C(15)	1.350 (7)
C(15)-C(25)	1.494 (8)
O(17)-C(20)	1.337 (7)
C(19)-C(22)	1.492 (8)
O(1)-C(14)	1.411 (6)
C(2)-C(10)	1.387 (7)
O(3)-C(13)	1.353 (6)
O(5)-C(11)	1.216 (6)
C(6)-C(20)	1.387 (8)
C(7)-C(13)	1.415 (7)
C(7)-C(21)	1.468 (8)
C(8)-C(24)	1.492 (8)
O(12)-C(21)	1.320 (7)
C(13)-C(15)	1.402 (8)
C(14)-C(16)	1.378 (7)
C(16)-C(19)	1.383 (8)
C(18)-C(20)	1.375 (8)
O(23)-C(26)	1.250 (8)

Table B.6 Bond angles (°) for atranorin.

C(11)-O(1)-C(14)	117.7(4)
C(8)-C(2)-C(11)	124.2(4)
C(10)-C(6)-C(20)	116.9(5)
C(20)-C(6)-C(26)	122.6(5)
C(13)-C(7)-C(21)	116.1(4)
C(2)-C(8)-C(18)	119.3(4)
C(18)-C(8)-C(24)	116.0(5)
C(2)-C(10)-C(6)	121.1(5)
O(1)-C(11)-C(2)	114.4(4)
C(2)-C(11)-O(5)	124.6(4)
O(3)-C(13)-C(7)	123.1(4)
C(7)-C(13)-C(15)	122.5(5)
O(1)-C(14)-C(16)	116.3(4)
C(13)-C(15)-C(14)	115.0(5)
C(14)-C(15)-C(25)	124.0(5)
C(8)-C(18)-C(20)	121.2(5)
C(7)-C(19)-C(22)	125.1(4)
C(6)-C(20)-O(17)	120.6(5)
O(17)-C(20)-C(18)	117.5(5)
C(7)-C(21)-O(12)	114.6(4)
C(6)-C(26)-O(23)	122.4(6)
C(8)-C(2)-C(10)	119.5(4)
C(10)-C(2)-C(11)	116.2(4)
C(10)-C(6)-C(26)	120.6(5)
C(13)-C(7)-C(19)	119.3(4)
C(19)-C(7)-C(21)	124.6(4)
C(2)-C(8)-C(24)	124.6(4)
C(2)-C(10)-O(4)	123.1(4)
O(4)-C(10)-C(6)	115.8(4)
O(1)-C(11)-O(5)	121.0(4)
C(21)-O(12)-C(27)	117.4(4)
O(3)-C(13)-C(15)	114.4(4)
O(1)-C(14)-C(15)	118.5(4)
C(15)-C(14)-C(16)	124.9(5)
C(13)-C(15)-C(25)	121.0(5)
C(14)-C(16)-C(19)	120.4(5)
C(7)-C(19)-C(16)	117.8(4)
C(16)-C(19)-C(22)	117.0(4)
C(6)-C(20)-C(18)	121.9(5)
C(7)-C(21)-O(9)	123.5(5)
O(9)-C(21)-O(12)	121.9(5)

Table B.7 Anisotropic displacement coefficients ($Å^2x10^3$) for atranorin. The standard deviation of the least significant figure of each distance is given in parentheses.

	U_{11}	U_{22}	U_{33}	U_{12}	U_{13}	U_{23}
O(1)	77(2)	34(2)	74(2)	15(2)	22(2)	13(2)
C(2)	37(3)	28(3)	60(3)	0(2)	-4(2)	-1(3)
O(3)	60(2)	50(2)	91(3)	-7(2)	-6(2)	3(2)
O(4)	76(3)	50(2)	87(3)	19(2)	18(2)	4(2)
O(5)	68(2)	56(3)	83(3)	14(2)	26(2)	15(2)
C(6)	58(4)	28(4)	76(4)	3(3)	-21(3)	-3(3)
C(7)	47(3)	38(4)	52(3)	4(2)	14(2)	-3(3)
C(8)	42(3)	36(3)	68(3)	2(2)	-4(3)	8(3)
O(9)	89(3)	37(2)	85(3)	-10(2)	4(2)	3(2)
C(10)	41(3)	51(4)	59(3)	5(3)	-5(3)	-5(3)
C(11)	38(3)	40(4)	62(3)	4(2)	-1(3)	-3(3)
O(12)	101(3)	44(2)	76(3)	4(2)	-12(2)	12(2)
C(13)	39(3)	41(4)	64(3)	0(2)	12(3)	-4(3)
C(14)	51(3)	38(4)	62(3)	7(3)	22(3)	4(3)
C(15)	41(3)	50(4)	61(3)	6(3)	8(3)	3(3)
C(16)	63(3)	46(4)	58(3)	-1(3)	2(3)	-8(3)
O(17)	89(3)	50(3)	110(3)	-8(2)	-21(2)	15(2)
C(18)	47(3)	65(4)	72(3)	-6(3)	-9(3)	9(3)
C(19)	64(3)	31(3)	54(3)	3(2)	3(3)	-1(3)
C(20)	59(4)	28(4)	83(4)	-15(3)	-22(3)	15(3)
C(21)	57(4)	42(4)	56(3)	9(3)	13(3)	0(3)
C(22)	118(5)	50(4)	78(4)	-10(3)	-27(4)	-1(3)
O(23)	109(3)	44(3)	135(4)	16(2)	-32(3)	-1(2)
C(24)	66(3)	71(4)	77(4)	14(3)	24(3)	21(3)
C(25)	62(3)	75(4)	88(4)	9(3)	-8(3)	8(3)
C(26)	81(4)	56(4)	104(5)	10(4)	-26(3).	-10(4)
C(27)	142(6)	65(4)	79(4)	10(4)	-6(4)	22(3)

The anisotropic displacement exponent takes the form:

$-2\pi^2(h^2a^{*2}U_{11} + \ldots + 2hka^*b^*U_{12})$

Table B.8 Proton-atom coordinates ($x10^4$) and isotropic displacement coefficients ($Å^2x10^3$) for atranorin. The standard deviation of the least significant figure of each distance is given in parentheses.

	x	y	z	U
H(3A)	1015	4196	1572	80
H(4A)	-85	9073	1813	80
H(16A)	3045	7276	2093	80
H(17A)	974	11776	121	80
H(18A)	2396	10065	-441	80
H(22A)	3972	6585	2945	80
H(22B)	3333	5852	3355	80
H(22C)	4244	5601	2800	80
H(24A)	3008	8730	-466	80
H(24B)	3145	8292	281	80
H(24C)	2190	7995	-226	80
H(25A)	577	6708	352	80
H(25B)	836	5727	186	80
H(25C)	-164	5970	676	80
H(26A)	-519	11101	1479	80
H(27A)	3669	3590	3727	80
H(27B)	2448	3337	3544	80
H(27C)	3401	3110	3012	80